NTNU
Kunnskap for en bedre verden

KANDIDAT
10043

PRØVE
TTK4550 1 Teknisk kybernetikk, fordypningsprosjekt

Emnekode	TTK4550
Vurderingsform	Arbeider
Starttid	20.08.2018 07:00
Sluttid	18.12.2018 22:59
Sensurfrist	18.01.2019 23:59
PDF opprettet	08.07.2019 11:19

Seksjon 1

Oppgave	Tittel	Oppgavetype
1	Ny oppgave	Filopplasting
2	Ny oppgave	Filopplasting

1 Ny oppgave

1. Prosjektoppgave

Last opp din prosjektoppgave her.

Din fil ble lastet opp og lagret i besvarelsen din.

Last ned | Fjern | Erstatt

Filnavn:	Prosjektoppgave.pdf
Filtype:	application/pdf
Filstørrelse:	13.56 MB
Opplastingstidspunkt:	18.12.2018 20:14
Status:	**Lagret**

2 # Ny oppgave

2. Eventuelt vedlegg

Last opp eventuelle vedlegg til prosjektoppgaven her.

Din fil ble lastet opp og lagret i besvarelsen din.

Last ned | Fjern | Erstatt

Filnavn:	Matlab-files.zip
Filtype:	application/x-zip-compressed
Filstørrelse:	6.13 KB
Opplastingstidspunkt:	18.12.2018 20:14
Status:	**Lagret**

NORWEGIAN UNIVERSITY OF SCIENCE AND TECHNOLOGY

TTK4550 SPECIALIZATION PROJECT

Analysis of Wireless Power Transfer Systems

Author:
Ernst TORSGÅRD

Supervisor:
Jon Are Wold SUUL

December 18, 2018

Faculty of Information Technology and Electrical Engineering
Department of Engineering Cybernetics

Abstract

Inductive power transfer (IPT) is an emerging technology adopted in a myriad of applications, ranging from wireless charging of mobile phones to more high-power applications such as wireless battery charging of electric vehicles.

A nonlinear state-space representation for a series-series compensated inductive power transfer system has been analyzed in this report. This model is represented in a synchronous reference frame (SRF) in order for every state variable to reach a constant value in a steady-state condition, thus allowing for linearization. The linearized state-space model describes the small-signal dynamics of the IPT-system and can represent a constant voltage load (CVL) conditions on the vehicle side. This model serves as a foundation for investigating various stability properties and control theory measures.

Analysis of the controllability Gramian has provided insight into how controllable the developed model is with different input configurations. Certain input variables have been determined to only give a minor contribution to overall controllability, whereas some others have a bigger impact. This examination has also provided understanding in which side of the IPT-system, the sending or the receiving side, to actuate in order to achieve the best controllability. Similarly, investigation of the observability Gramian has revealed how observable the system is with different output configurations. Eigenvalue analysis of the system has shown that there exists a pole pair, a critical mode, with notable lower damping and longer settling time than the others. Thus, participation factors have been investigated in order to determine which states that participate most in the critical mode. Furthermore, analysis of transfer functions has made awareness in the possibilities of model order reduction, which could simplify further analysis and potential of control design.

Table of Contents

List of Tables

List of Figures

Abbreviations

EV	=	**E**lectrical **V**ehicle
IPT	=	**I**nductive **P**ower **T**ransfer
KVL	=	**K**irchoff's **V**oltage **L**aw
SRF	=	**S**ynchronous **R**eference **F**rame
TF	=	**T**ransfer **F**unction

Chapter 1

Introduction and Motivation

Electricity-based transportation is a field of research which has gained increasing attention over the last decades. Inductive power transfer (IPT) is a technology which transfers electrical energy from a power source to an electrical device without any wires or other kinds of conductors as a physical link and could help accelerate the transition from regular petroleum-based vehicles to zero-emission vehicles[2][3].

The recent years have shown a huge rise in popularity for electric vehicles (EV). Some obvious reasons for this are technological advances such as the development of electrical energy storage systems with increasing energy and power densities, which reduces limitations in aspects such as driving range per recharge, and the fact that EV's are getting more high-technological and advanced[4]. The gap between EV's and fossil-fueled cars in terms of driving comfort and safety is decreasing, and the increasing media attention for climate changes and global warming makes people more environmentally conscious. In addition, advancements in technology reduce the production costs of EV's, and they are therefore more accessible to the general public[2][3]. As well as being cheap to drive due to electricity being less expensive than fossil-fuel, several governments propose incentives such as exemption from road taxes, reduced yearly fees and free public charging stations[5], thus making EV's more attractive. Another advantage of EV's is that they do not make a lot of noise in idle, or even when accelerating, compared to vehicles with internal combustion engines.

IPT is a battery charging concept which could greatly reduce barriers, such as limited driving range. To transfer wireless power from a charging system integrated into the road surface to a receiver coil mounted on the undercarriage of the EV, thus charging the onboard batteries without any physical contact, considerably simplifies the charging process and reduces safety issues, such as handling of the charging equipment[4]. Likewise, for marine applications, transferring wireless power from a dock-mounted inductive coupler to a marine vessel while docking could provide many of the same advantages[6]. However, there are still numerous improvements required in order to reduce and eliminate challenges that prevent this technology from an extensive and worldwide application. The purpose of this report is to investigate stability properties on a system for inductive power transfer, while considering the need for a more sustainable and efficient eco-friendly way of transportation.

1.1 Inductive power transfer

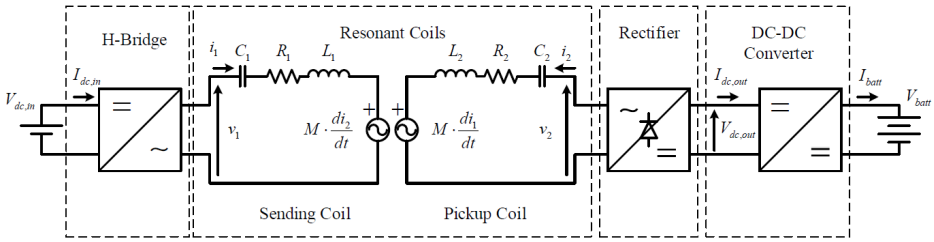

Figure 1.1: Typical model for IPT-system [1]

A typical structure of an IPT-model is shown in Figure 1.1. It consists of an H-bridge converter on the sending side, two magnetically coupled coils, a diode rectifier and a dc-dc converter on the receiving side. However, other topologies are possible as well, depending on their application and desired level of complexity and cost.

The functioning of the IPT-system is reminiscent of the functioning of more familiar transformers. The main idea is the same: Two coils with a mutual inductance between them, and when magnetically coupled, a current in one coil induces a voltage in the other coil without any physical contact – by the laws of Faraday

and Ampere. The primary side is energized by a power supply which in turn generates a magnetic field, a pickup system extracts the magnetically coupled power from the primary side and a rectifier on the secondary side producing a dc output voltage[1][2][3][7].

As mentioned, electric vehicles have gained a lot of popularity in the last decades. This kind of transportation has a clear environmental advantage on cars with engines fueled by gasoline or diesel, which contribute significantly to greenhouse gasses. Today's EV's are on the same level as vehicles with internal combustion engines in almost all aspects, e.g. driving comfort, acceleration, etc. In fact, they are even more efficient, more accurate and have faster torque response[4]. However, this emission-free transportation method has some limitations that need to be addressed. The need for costly and quite bulky and heavy energy storage system onboard – batteries – in order to have workable mileage range per recharge is one of those. Dynamical charging reduces these drawbacks significantly. IPT-technology could make it possible to transfer power and to charge EV's even while they are in motion. There is no longer need for such large energy storage systems onboard with the use of this technology, which would make the electrical vehicles lighter and even more efficient. Another advantage is that IPT-technology eliminates the needs of a physical link while recharging the battery, which is important regarding safety, and makes the overall recharging process easy and convenient since it is fully automated. In addition, IPT is clean and unaffected by dirt and other external influences like chemicals and weather, i.e. the technology is tolerant in quite harsh conditions[2].

1.2 Challenges and difficulties of IPT-systems

Depending on their application, inductive power transfer systems can be subdivided into two main groups: dynamic and static IPT. Dynamic IPT refers to in-motion charging of EV', whereas static IPT refers to stationary charging of EV's. The challenges that arise in static IPT also arises in dynamic IPT. However, the latter is subject to more difficulties, and a short summary of the challenges in both cases are presented below.

A huge challenge in IPT-design for dynamic power transfer is the large and pos-

sibly varying air gap between the transmitter and receiver and the frequently occurring misalignment. In IPT-systems for land-based EV's, the air gap between the road and the pad receiving power underneath the car is clearly quite high compared other systems using the same functionality, e.g. transformers, thus lowering the magnetic coupling and efficiency. And, in addition, the track system in the ground has to be covered with a layer of asphalt or some other kind of material used in road construction, making the gap even larger. Similarly, a ship docked at the harbor is exposed to waves and tide and will therefore drift and move relative to the dock-mounted coupler. Moreover, the loading or unloading of ship cargo will affect the displacement and buoyancy of the vessel – and consequently the air draft[6]. Due to this, weak magnetic coupling becomes a difficulty for IPT-systems. Therefore, the main focus in the construction of IPT-systems is to enhance the tolerance to misalignment and the resulting variation of the magnetic coupling by improving the magnetic design and control of power[2]. It is clear that an IPT-system has several parameters which could vary during in-motion dynamic charging, e.g. coupling factor and mutual inductance due to the variation in the air gap, variation in load and misalignment. To deal with such parameter variation, good controllability is needed[8]. Reduction in the variation of the magnetic coupling can be achieved by the use of larger coils, however, this increases expenses and counteracts the realization of compact systems, which is undesirable.

1.3 Series-series compensation

As mentioned, wireless charging of marine vessels and land-based EV's entails a notable and varying air gap between the sending and pickup coil due to e.g. waves, tide, unevenness in the road structure and the need for adequate clearance between the road surface and the EV. In addition, a marine vessel or an electric vehicle in motion will always cause some misalignment. These constraints weaken the mutual coupling and cause a high leakage inductance, which leads to poor efficiency. It is therefore very important to choose a suitable compensation scheme when designing an IPT-system. Conditions like maximum efficiency, output power independent of both load and coupling coefficient and so on need to be considered[9]. To cope with these challenges requires the introduction of capacitive compensation in both sending and pickup coil[10].

The compensation topology considered in this report is the series-series compen-

sation, as shown in Figure 1.1, that is, both primary and secondary coils are series compensated. This topology can act as a constant current source, which is necessary when charging a battery. In addition, the resonant frequency of this structure is only subject to minor variations due to varying load and magnetic coupling conditions under operation[11], which is an important advantage. Moreover, it is very effective when there is no misalignment[10][12][13].

1.4 Constant voltage load

Constant voltage load (CVL) is a model characteristic where the output voltage of the system on the load resistance is modeled as constant, regardless of the value of the load. The developed model will include this condition since studies have shown that representing the load as an equivalent resistant do not capture the dynamic behavior a constant voltage source generates[1][11].

1.5 Objectives

This research has focused on analyzing a linearizable model for an inductive power transfer system accurately capturing constant voltage load conditions at the receiving side, and to investigate control measures and stability properties of this model.

1.6 Outline

This report is structured as follows:

- *Chapter 1* gives an introduction to IPT-technology and provides information on important concepts and what challenges this technology faces.
- *Chapter 2* presents relevant background theory for this report.
- *Chapter 3* displays the derivation and linearization of a nonlinear model describing the dynamics of an IPT-system.
- *Chapter 4* provides results and discussion of the analyzed stability and sensitivity properties.

- *Chapter 5* provides results and discussion of the analyzed Gramians.
- *Chapter 6* issues concluding remarks and suggestions for future work.

Chapter 2

Background Theory

2.1 Linear state-space representation

The dynamics of a linear and time-invariant system are described in state-space representation as:

$$\begin{aligned} \dot{\boldsymbol{x}}(t) &= \boldsymbol{A}\boldsymbol{x}(t) + \boldsymbol{B}\boldsymbol{u}(t) \\ \boldsymbol{y}(t) &= \boldsymbol{C}\boldsymbol{x}(t) \end{aligned} \tag{2.1}$$

where $\boldsymbol{x}(t) \in \mathbb{R}^n$ are the states, $\boldsymbol{u}(t) \in \mathbb{R}^p$ are the control inputs and $\boldsymbol{y}(t) \in \mathbb{R}^q$ are the outputs of the model. The state matrix $\boldsymbol{A} \in \mathbb{R}^{n\times n}$, input matrix $\boldsymbol{B} \in \mathbb{R}^{n\times p}$ and output matrix $\boldsymbol{C} \in \mathbb{R}^{q\times n}$ are constant matrices.

2.2 Nonlinear state-space representation

The dynamics of a state-space model of a nonlinear system are described by:

$$\begin{aligned} \dot{\boldsymbol{x}}(t) &= \boldsymbol{f}(\boldsymbol{x}, \boldsymbol{u}) \\ \boldsymbol{y}(t) &= \boldsymbol{g}(\boldsymbol{x}, \boldsymbol{u}) \end{aligned} \tag{2.2}$$

where $\boldsymbol{f} \in \mathbb{R}^n$ and $\boldsymbol{g} \in \mathbb{R}^l$ are vectors of functions describing the nonlinear model.

2.3 Controllability

Controllability refers to the ability of a controller to alter the functionality of a system.

Theorem Controllability:

The state equation 2.1 or the pair $(\boldsymbol{A}, \boldsymbol{B})$ is said to be controllable if for any initial state $\boldsymbol{x}(0) = \boldsymbol{x}_0$ and any final state $\boldsymbol{x}_1$, there exists and input $\boldsymbol{u}(\cdot)$ that transfer $\boldsymbol{x}_0$ to $\boldsymbol{x}_1$ in a finite time. Otherwise, the pair $(\boldsymbol{A}, \boldsymbol{B})$ is said to be uncontrollable[14]. Kalman's controllability matrix reads:

$$\boldsymbol{\mathcal{C}} = [\boldsymbol{B} \quad \boldsymbol{AB} \quad \boldsymbol{A}^2\boldsymbol{B} \ \ldots \ \boldsymbol{A}^{n-1}\boldsymbol{B}] \tag{2.3}$$

and Kalman's rank criterion states that the rank of this controllability matrix needs to be n, i.e. have full row rank, for the system to be controllable. This binary rank condition only states whether the system is completely controllable or not, and do not say anything in what way the system is or is not controllable or how much input energy which is required to steer the system around in the state-space. It is, however, relevant to consider more quantitative measures of controllability. The controllability Gramian handles this matter, as seen in the next section.

2.4 Controllability Gramian

The symmetric positive semidefinite matrix:

$$\boldsymbol{W}_c(t) = \int_0^t e^{\boldsymbol{A}\tau}\boldsymbol{B}\boldsymbol{B}^T e^{\boldsymbol{A}^T\tau} d\tau \in \mathbb{R}^{n\times n} \tag{2.4}$$

is called the controllability Gramian at time t. The eigenvectors and eigenvalues of this matrix are the vectors $\boldsymbol{\xi}$ and the roots λ of the characteristic polynomial of $\boldsymbol{W}_c(t)$ such that:

$$\boldsymbol{W}_c\boldsymbol{\xi} = \lambda\boldsymbol{\xi} \tag{2.5}$$

The eigenvectors corresponding to the largest eigenvalues of the Gramian are the most controllable directions in the state-space $\boldsymbol{x}(t) \in \mathbb{R}^n$. This means that it is possible to go further in the directions of the eigenvectors corresponding to larger eigenvalues than it is possible in the directions spanned by eigenvectors with a corresponding smaller eigenvalue – using the same amount of input energy. Thus this matrix provides an energy-related quantification of controllability; it describes how much energy that is required to move the system around in the state-space[15][16].

For stable systems, there exists a finite positive definite Gramian defined by:

$$\boldsymbol{W}_c = \int_0^\infty e^{\boldsymbol{A}\tau}\boldsymbol{B}\boldsymbol{B}^T e^{\boldsymbol{A}^T\tau} d\tau \in \mathbb{R}^{n\times n} \tag{2.6}$$

which can easily be found by solving the Lyapunov equation:

$$\boldsymbol{A}\boldsymbol{W}_c + \boldsymbol{W}_c\boldsymbol{A}^T = -\boldsymbol{B}\boldsymbol{B}^T \tag{2.7}$$

The controllable directions, i.e the eigenvectors, and the eigenvalues of this matrix defines an energy ellipsoid in $\mathbb{R}^n$ which describes the surface of how far in any direction it is possible to steer the system with a unit or less of input energy, i.e.:

$$\mathcal{E}_{min} = \{\boldsymbol{x} \in \mathbb{R}^n \mid \boldsymbol{x}^T\boldsymbol{W}_c^{-1}\boldsymbol{x} \leq 1\} \tag{2.8}$$

From this controllability Gramian, there exist several different ways to quantify and interpret the controllability:
1) The trace of the Gramian, $tr(\boldsymbol{W}_c)$. It can be interpreted as the average controllability in all of the directions in state-space, as it is inversely related to the average energy needed to move the system around. If the system is uncontrollable, the average energy is infinity because there exists at least one direction of which it is impossible to drive the system using the control inputs.
2) The determinant of the Gramian, $det(\boldsymbol{W}_c)$. It is related to the volume enclosed by the ellipsis it defines:

$$V(\mathcal{E}_{min}) = \frac{\pi^{\frac{n}{2}}}{\Gamma(\frac{n}{2}+1)} \sqrt[n]{det(\boldsymbol{W}_c)} \tag{2.9}$$

where Γ is the gamma function. That is, the determinant is a measure of the set of states that can be reached with one unit or less of input energy. However, computing the determinant could be problematic when the states n grows large, so it is common to consider the logarithm of the determinant instead, $log(det(\boldsymbol{W}_c))$. If the system is uncontrollable, this volume would be zero.
3) The smallest eigenvalue of the Gramian, $min\{\lambda_1 \ \dots \ \lambda_n\}$. As described earlier, this measure is inversely related to the amount of energy required to move the system in the direction of the state-space that is most difficult to control. That is, the smaller the eigenvalue, the more energy needed.
4) The eigenvector corresponding to the smallest eigenvalue. This is the direction which requires most input energy to steer the system in, compared to all other directions in the n-dimensional state-space. The eigenvectors span the controllable subspace, and the corresponding eigenvalues can be interpreted as the length of the eigenvector.
5) The rank of the Gramian, $rank(\boldsymbol{W}_c)$. This is the dimension of the controllable subspace[15][16].

2.5 Observability

Observability refers to the ability of estimating any state $\boldsymbol{x}(t)$ from the measurement $\boldsymbol{y}(t)$.

Theorem Observability:

The state equation 2.1 is said to be controllable if for any unknown initial state $\boldsymbol{x}(0)$, there exists a finite $t_1 > 0$ such that knowledge of the input $\boldsymbol{u}$ and the output $\boldsymbol{y}$ over $[0, t_1]$ suffices to determine uniquely the initial state $\boldsymbol{x}(0)$. Otherwise the system is said to be unobservable[14]. Kalman's observability matrix reads:

$$\boldsymbol{\mathcal{O}} = [\boldsymbol{C} \quad \boldsymbol{CA} \quad \boldsymbol{CA}^2 \ \dots \ \boldsymbol{CA}^{n-1}]^T \tag{2.10}$$

and Kalman's rank criterion states that the rank of this observability matrix needs

to be n, i.e. have full column rank, for the system to be observable. Similarly, as for the controllability property, this is also a binary rank condition and do not say anything in what way the system is or is not observable. Therefore, the more quantitative observability Gramian matrix has been introduced to handle this matter as well.

2.6 Observability Gramian

The symmetric positive semidefinite matrix:

$$\boldsymbol{W}_o(t) = \int_0^t e^{\boldsymbol{A}\tau}\boldsymbol{C}^T\boldsymbol{C}e^{\boldsymbol{A}^T\tau}d\tau \in \mathbb{R}^{n\times n} \tag{2.11}$$

is called the observability Gramian at time t. The eigenvectors and eigenvalues of this matrix are the vectors $\boldsymbol{\xi}$ and the roots λ of the characteristic polynomial of $\boldsymbol{W}_o(t)$ such that:

$$\boldsymbol{W}_o\boldsymbol{\xi} = \lambda\boldsymbol{\xi} \tag{2.12}$$

For stable systems, there exists a finite positive definite Gramian defined by:

$$\boldsymbol{W}_o = \int_0^\infty e^{\boldsymbol{A}\tau}\boldsymbol{C}^T\boldsymbol{C}e^{\boldsymbol{A}^T\tau}d\tau \in \mathbb{R}^{n\times n} \tag{2.13}$$

which can easily be found by solving the Lyapunov equation:

$$\boldsymbol{A}\boldsymbol{W}_o + \boldsymbol{W}_o\boldsymbol{A}^T = -\boldsymbol{C}^T\boldsymbol{C} \tag{2.14}$$

Controllability and observability are dual properties, thus, all measures and interpretations of the controllability Gramian hold for the observability Gramian as well – albeit describing the degree of observability in the latter case. [15][16].

2.7 Participation factors

The participation factors is a tool for analyzing the level of interaction between the states and the modes of a linear time-invariant system. It is a method of quantifying the degree of connection a system variable have in a system mode, which makes it possible to determine which state variables that are most relevant for a particular mode. That is, the participation factor is a measure of eigenvalue sensitivity. This approach could simplify the analysis of the system, since, instead of looking into the entire model, the main focus could lie on the state variables which interacts most with the critical modes[17].

There exist several different approaches to compute the participation factors for a linear time-invariant system. In this report, four methods have been explored, and the different formulas for calculating the participation factor p_{ki} of the state x_k in the i-th mode are as follows[17][18]:

Method I:

$$p_{ki} = l_k^i r_k^i \tag{2.15}$$

Method II:

$$p_{ki} = \frac{(\Re\{l_k^i\})^2}{\Re\{l^i\}(\Re\{l^i\})^T} \tag{2.16}$$

Method III:

$$p_{ki} = \frac{|l_k^i|^2}{\sum_{j=1}^{n} |l_j^i|} \tag{2.17}$$

Method IV:

$$p_{ki} = 2\Re\{l_k^i r_k^i\}) \tag{2.18}$$

where l^i and r^i are respectively the left and right eigenvectors of the matrix $\boldsymbol{A}$ in 2.1 associated with the eigenvalues λ_i for $i \in 1 \dots n$, and l_k^i and r_k^i are the k-th

index of the i-th eigenvector.

Chapter 3

Nonlinear Model and Linearization

3.1 Large-signal IPT-model

3.1.1 State-space representation of circuit

The differential equations describing the dynamics of the system in Figure 1.1 can be obtained by applying Kirchoff's voltage law (KVL) around the sending- and pickup coil:

$$v_1 = R_1 i_1 + L_1 \frac{di_1}{dt} + M \frac{di_2}{dt} + v_{C1} \tag{3.1a}$$

$$v_2 = R_2 i_2 + L_2 \frac{di_2}{dt} + M \frac{di_1}{dt} + v_{C2} \tag{3.1b}$$

$$\frac{dv_{C_1}}{dt} = \frac{1}{C_1} i_1 \tag{3.1c}$$

$$\frac{dv_{C_2}}{dt} = \frac{1}{C_2} i_2 \tag{3.1d}$$

All variables of this model will be time-periodic when reached steady-state. This hinders the model to be represented in a state-space formulation where the state variables arrive at a constant value when evaluated at the equilibrium point. To conduct stability analysis such as examination of eigenvalues, a steady-state time-

invariant state-space representation is required. In order to obtain a such linearizable state-space representation of this model, it is transformed into a synchronously rotating reference frame (SRF) by application of the Park transformation.

Expressing the model with the derivatives of the state variables on the left-hand side, i.e. solving equations 3.1a and 3.1b for the derivatives of the current, results in:

$$\frac{di_1}{dt} = \frac{1}{L_1}(v_1 - R_1 i_1 - v_{C1} - M\frac{di_2}{dt}) \tag{3.2a}$$

$$\frac{di_2}{dt} = \frac{1}{L_2}(v_2 - R_2 i_2 - v_{C2} - M\frac{di_1}{dt}) \tag{3.2b}$$

These two equations are connected due to the mutual coupling between the coils, that is, the derivative of the current in the sending coil shows up in the equation describing the dynamics of the pickup coil, and vice versa. Therefore, substituting equation 3.2b in 3.2a, gives:

$$\begin{aligned}
&\frac{di_1}{dt} = \frac{1}{L_1}(v_1 - R_1 i_1 - v_{C1} - \frac{M}{L_2}(v_2 - R_2 i_2 - v_{C2} - M\frac{di_1}{dt})) \\
&\Rightarrow \frac{di_1}{dt}(1 - \frac{M^2}{L_1 L_2}) = \frac{1}{L_1}(v_1 - R_1 i_1 - v_{C1} - \frac{M}{L_2}v_2 + \frac{MR_2}{L_2}i_2 + \frac{M}{L_2}v_{C2}) \\
&\Rightarrow \frac{di_1}{dt} = \frac{1}{L_1 - \frac{M^2}{L_2}}(v_1 - R_1 i_1 - v_{C1} - \frac{M}{L_2}v_2 + \frac{MR_2}{L_2}i_2 + \frac{M}{L_2}v_{C2}) \\
&\Rightarrow \frac{di_1}{dt} = -\frac{R_1}{L_{\alpha 1}}i_1 + \frac{MR_2}{L_{\alpha 1}L_2}i_2 - \frac{1}{L_{\alpha 1}}v_{C1} + \frac{M}{L_{\alpha 1}L_2}v_{C2} + \frac{1}{L_{\alpha 1}}v_1 - \frac{M}{L_{\alpha 1}L_2}v_2
\end{aligned} \tag{3.3a}$$

Applying the same procedure for equation 3.2b, i.e. substituting equation 3.2a in equation 3.2b yields:

$$\frac{di_2}{dt} = \frac{MR_1}{L_{\alpha 2}L_1}i_1 - \frac{R_2}{L_{\alpha 2}}i_2 + \frac{M}{L_{\alpha 2}L_1}v_{C1} - \frac{1}{L_{\alpha 2}}v_{C2} - \frac{M}{L_{\alpha 2}L_1}v_1 + \frac{1}{L_{\alpha 2}}v_2 \tag{3.4}$$

with the leakage factors defined as:

$$
\begin{aligned}
L_{\alpha 1} &= L_1 - \frac{M^2}{L_2} \\
L_{\alpha 2} &= L_2 - \frac{M^2}{L_1}
\end{aligned}
\tag{3.5}
$$

3.1.2 SRF and dq-coordinates

The systems operating frequency is defined by ω, which is related to the angle θ through the equality $\theta = \omega t$. Then, applying the Park transformation, i.e. transforming the model into a synchronously rotating reference frame defined by $x_{dq} = x \cdot e^{-j\theta}$ with $\theta = \omega t$, by multiplying both sides of equation 3.3a with the term $e^{-j\theta}$, results in:

$$
\begin{aligned}
\frac{di_1}{dt} \cdot e^{-j\theta} = &-\frac{R_1}{L_{\alpha 1}} \underbrace{i_1 \cdot e^{-j\theta}}_{i_{1,dq}} + \frac{MR_2}{L_{\alpha 1} L_2} \underbrace{i_2 \cdot e^{-j\theta}}_{i_{2,dq}} - \frac{1}{L_{\alpha 1}} \underbrace{v_{C1} \cdot e^{-j\theta}}_{v_{C1,dq}} + \frac{M}{L_{\alpha 1} L_2} \underbrace{v_{C2} \cdot e^{-j\theta}}_{v_{C2,dq}} \\
&+ \frac{1}{L_{\alpha 1}} \underbrace{v_1 \cdot e^{-j\theta}}_{v_{1,dq}} - \frac{M}{L_{\alpha 1} L_2} \underbrace{v_2 \cdot e^{-j\theta}}_{v_{2,dq}}
\end{aligned}
\tag{3.6}
$$

By noting that $x_{dq} = x \cdot e^{-j\theta} \iff x = x_{dq} \cdot e^{j\theta}$ and that $\theta = \omega t$, it is possible to treat the derivative term on the left hand side:

$$
\begin{aligned}
\frac{di_1}{dt} \cdot e^{-j\theta} &= (\frac{d}{dt}(i_{1,dq} \cdot e^{j\omega t}))e^{-j\omega t} \\
&= (\frac{di_{1,dq}}{dt} e^{j\omega t} + j\omega \cdot i_{1,dq} \cdot e^{j\omega t})e^{-j\omega t} \\
&= \frac{di_{1,dq}}{dt} + j\omega \cdot i_{1,dq}
\end{aligned}
\tag{3.7}
$$

Combining these above results, a differential vector equation describing the current on the sending side arises:

$$\begin{aligned}\frac{di_{1,dq}}{dt} =& - j\omega \cdot i_{1,dq} - \frac{R_1}{L_{\alpha 1}} \cdot i_{1,dq} + \frac{MR_2}{L_{\alpha 1}L_2} \cdot i_{2,dq} - \frac{1}{L_{\alpha 1}} \cdot v_{C1,dq} \\ &+ \frac{M}{L_{\alpha 1}L_2} \cdot v_{C2,dq} \frac{1}{L_{\alpha 1}} \cdot v_{1,dq} - \frac{M}{L_{\alpha 1}L_2} \cdot v_{2,dq}\end{aligned} \tag{3.8}$$

Similar procedure for 3.2b, i.e. applying the Park transformation, results in a differential vector equation describing the current on the receiving side:

$$\begin{aligned}\frac{di_{2,dq}}{dt} =& - j\omega \cdot i_{2,dq} + \frac{MR_1}{L_{\alpha 2}L_1} \cdot i_{1,dq} - \frac{R_2}{L_{\alpha 2}} \cdot i_{2,dq} + \frac{M}{L_{\alpha 2}L_1} \cdot v_{C1,dq} \\ &- \frac{1}{L_{\alpha 2}} \cdot v_{C2,dq} - \frac{M}{L_{\alpha 2}L_1} \cdot v_{1,dq} + \frac{1}{L_{\alpha 2}} \cdot v_{2,dq}\end{aligned} \tag{3.9}$$

Furthermore, applying the dq-transformation on the last two equations of the model, equations 3.1c and 3.1d, results in:

$$\frac{dv_{C1}}{dt} \cdot e^{-j\theta} = \frac{1}{C_1} i_1 \cdot e^{-j\theta} \tag{3.10a}$$

$$\frac{dv_{C2}}{dt} \cdot e^{-j\theta} = \frac{1}{C_2} i_2 \cdot e^{-j\theta} \tag{3.10b}$$

Treating the derivative terms in a similar way as before:

$$\begin{aligned}\frac{dv_{C1}}{dt} \cdot e^{-j\theta} &= (\frac{d}{dt}(v_{C1,dq} \cdot e^{j\omega t}))e^{-j\omega t} \\ &= (\frac{dv_{C1,dq}}{dt} \cdot e^{j\omega t} + j\omega \cdot v_{C1,dq} \cdot e^{j\omega t})e^{-j\omega t} \\ &= \frac{dv_{C1,dq}}{dt} + j\omega \cdot v_{C1,dq}\end{aligned} \tag{3.11}$$

and:

$$\begin{aligned}\frac{dv_{C2}}{dt}\cdot e^{-j\theta} &= (\frac{d}{dt}(v_{C2,dq}\cdot e^{j\omega t}))e^{-j\omega t}\\ &= (\frac{dv_{C2,dq}}{dt}\cdot e^{j\omega t} + j\omega\cdot v_{C2,dq}\cdot e^{j\omega t})e^{-j\omega t}\\ &= \frac{dv_{C2,dq}}{dt} + j\omega\cdot v_{C2,dq}\end{aligned} \tag{3.12}$$

the two differential vector equations describing the voltages across the capacitors at both sending- and pickup coil arises:

$$\frac{dv_{C1,dq}}{dt} = -j\omega\cdot v_{C1,dq} + \frac{1}{C_1}\cdot i_{1,dq} \tag{3.13a}$$

$$\frac{dv_{C2,dq}}{dt} = -j\omega\cdot v_{C2,dq} + \frac{1}{C_2}\cdot i_{2,dq} \tag{3.13b}$$

3.1.3 CVL-condition and nonlinearity

In order to represent the CVL-characteristic of the model, the voltage at the receiving side should be expressed such that it is determined by $V_{dc,out}$ and i_2. Therefore, the fundamental frequency component of the rectified voltage v_2 is [1]:

$$v_2 = -\frac{i_2}{I_2}\cdot\frac{4}{\pi}\cdot V_{dc,out} \tag{3.14}$$

where I_2 is the amplitude of i_2. In the dq-reference frame, the amplitude I_2 is the euclidean norm of the complex vector $i_{2,dq}$, i.e. $|i_{2,dq}| = \sqrt{i_{2,d}^2 + i_{2,q}^2}$. Thus, the voltage at the receiving side is expressed in dq-components as:

$$v_{2,dq} = -\frac{i_{2,dq}}{\sqrt{i_{2,d}^2 + i_{2,q}^2}}\cdot\frac{4}{\pi}\cdot V_{dc,out} \tag{3.15}$$

This introduces a nonlinearity in the model, which is now described by four nonlinear complex vector equations:

$$\begin{aligned}\frac{di_{1,dq}}{dt} =& - j\omega \cdot i_{1,dq} - \frac{R_1}{L_{\alpha 1}} \cdot i_{1,dq} + \frac{MR_2}{L_{\alpha 1}L_2} \cdot i_{2,dq} - \frac{1}{L_{\alpha 1}} \cdot v_{C1,dq} + \frac{M}{L_{\alpha 1}L_2} \cdot v_{C2,dq} \\ &+ \frac{1}{L_{\alpha 1}} \cdot v_{1,dq} + \frac{M}{L_{\alpha 1}L_2} \cdot \frac{i_{2,dq}}{\sqrt{i_{2,d}^2 + i_{2,q}^2}} \cdot \frac{4}{\pi} \cdot V_{dc,out}\end{aligned} \tag{3.16}$$

$$\begin{aligned}\frac{di_{2,dq}}{dt} =& - j\omega \cdot i_{2,dq} + \frac{MR_1}{L_{\alpha 2}L_1} \cdot i_{1,dq} - \frac{R_2}{L_{\alpha 2}} \cdot i_{2,dq} + \frac{M}{L_{\alpha 2}L_1} \cdot v_{C1,dq} - \frac{1}{L_{\alpha 2}} \cdot v_{C2,dq} \\ &- \frac{M}{L_{\alpha 2}L_1} \cdot v_{1,dq} - \frac{1}{L_{\alpha 2}} \cdot \frac{i_{2,dq}}{\sqrt{i_{2,d}^2 + i_{2,q}^2}} \cdot \frac{4}{\pi} \cdot V_{dc,out}\end{aligned} \tag{3.17}$$

$$\frac{dv_{C1,dq}}{dt} = -j\omega \cdot v_{C1,dq} + \frac{1}{C_1} \cdot i_{1,dq} \tag{3.18}$$

$$\frac{dv_{C2,dq}}{dt} = -j\omega \cdot v_{C2,dq} + \frac{1}{C_2} \cdot i_{2,dq} \tag{3.19}$$

3.1.4 General nonlinear state-space representation

Decomposing these equations and writing them on dq-form with $x_{dq} = x_d + jx_q$, the nonlinear state-space model is obtained, expressed in the general from $\dot{\boldsymbol{x}} = \boldsymbol{f}(\boldsymbol{x}, \boldsymbol{u})$ with the state- and input variables $\boldsymbol{x}$ and $\boldsymbol{u}$ defined as:

$$\boldsymbol{x} = \begin{bmatrix} i_{1,d} & i_{1,q} & i_{2,d} & i_{2,q} & v_{C1,d} & v_{C1,q} & v_{C2,d} & v_{C2,q} \end{bmatrix}^T \tag{3.20}$$

$$\boldsymbol{u} = \begin{bmatrix} v_{1,d} & v_{1,q} & \omega & V_{dc,out} \end{bmatrix}^T \tag{3.21}$$

The resulting nonlinear model of the system from Figure 1.1 is therefore given by:

$$\begin{aligned}\frac{di_{1,d}}{dt} =&\omega \cdot i_{1,q} - \frac{R_1}{L_{\alpha 1}} \cdot i_{1,d} + \frac{MR_2}{L_{\alpha 1}L_2} \cdot i_{2,d} - \frac{1}{L_{\alpha 1}} \cdot v_{C1,d} + \frac{M}{L_{\alpha 1}L_2} \cdot v_{C2,d} \\ &+ \frac{1}{L_{\alpha 1}} \cdot v_{1,d} + \frac{M}{L_{\alpha 1}L_2} \cdot \frac{i_{2,d}}{\sqrt{i_{2,d}^2 + i_{2,q}^2}} \cdot \frac{4}{\pi} \cdot V_{dc,out}\end{aligned} \tag{3.22}$$

$$\begin{aligned}\frac{di_{1,q}}{dt} =&-\omega \cdot i_{1,d} - \frac{R_1}{L_{\alpha 1}} \cdot i_{1,q} + \frac{MR_2}{L_{\alpha 1}L_2} \cdot i_{2,q} - \frac{1}{L_{\alpha 1}} \cdot v_{C1,q} + \frac{M}{L_{\alpha 1}L_2} \cdot v_{C2,q} \\ &+ \frac{1}{L_{\alpha 1}} \cdot v_{1,q} + \frac{M}{L_{\alpha 1}L_2} \cdot \frac{i_{2,q}}{\sqrt{i_{2,d}^2 + i_{2,q}^2}} \cdot \frac{4}{\pi} \cdot V_{dc,out}\end{aligned} \tag{3.23}$$

$$\begin{aligned}\frac{di_{2,d}}{dt} =&\omega \cdot i_{2,q} + \frac{MR_1}{L_{\alpha 2}L_1} \cdot i_{1,d} - \frac{R_2}{L_{\alpha 2}} \cdot i_{2,d} + \frac{M}{L_{\alpha 2}L_1} \cdot v_{C1,d} - \frac{1}{L_{\alpha 2}} \cdot v_{C2,d} \\ &- \frac{M}{L_{\alpha 2}L_1} \cdot v_{1,d} - \frac{1}{L_{\alpha 2}} \cdot \frac{i_{2,d}}{\sqrt{i_{2,d}^2 + i_{2,q}^2}} \cdot \frac{4}{\pi} \cdot V_{dc,out}\end{aligned} \tag{3.24}$$

$$\begin{aligned}\frac{di_{2,q}}{dt} =&-\omega \cdot i_{2,d} + \frac{MR_1}{L_{\alpha 2}L_1} \cdot i_{1,q} - \frac{R_2}{L_{\alpha 2}} \cdot i_{2,q} + \frac{M}{L_{\alpha 2}L_1} \cdot v_{C1,q} - \frac{1}{L_{\alpha 2}} \cdot v_{C2,q} \\ &- \frac{M}{L_{\alpha 2}L_1} \cdot v_{1,q} - \frac{1}{L_{\alpha 2}} \cdot \frac{i_{2,q}}{\sqrt{i_{2,d}^2 + i_{2,q}^2}} \cdot \frac{4}{\pi} \cdot V_{dc,out}\end{aligned} \tag{3.25}$$

$$\frac{dv_{C1,d}}{dt} = \omega \cdot v_{C1,q} + \frac{1}{C_1} \cdot i_{1,d} \tag{3.26}$$

$$\frac{dv_{C1,q}}{dt} = -\omega \cdot v_{C1,d} + \frac{1}{C_1} \cdot i_{1,q} \tag{3.27}$$

$$\frac{dv_{C2,d}}{dt} = \omega \cdot v_{C2,q} + \frac{1}{C_2} \cdot i_{2,d} \tag{3.28}$$

$$\frac{dv_{C2,q}}{dt} = -\omega \cdot v_{C2,d} + \frac{1}{C_2} \cdot i_{2,q} \tag{3.29}$$

3.2 Steady-state solutions

In order to perform eigenvalue analysis and to study stabilization properties like controllability and observability, it is necessary to linearize the model at an operating point defined by $\boldsymbol{f}(\boldsymbol{x}, \boldsymbol{u}) = 0$. The reference frame of the dq-model is defined to be synchronized with the peak amplitude of v_1. Therefore, q-axis voltage component at the sending side is zero, $v_{1,q,0} = 0$, and the d-axis voltage component is equal to the peak amplitude of v_1, $v_{1,d,0} = V_{1,0}$. Furthermore, it is assumed that the system operates at resonant frequency, i.e. $\omega = \omega_0$ [1].

Solving the equation $\boldsymbol{f}(\boldsymbol{x}, \boldsymbol{u}) = 0$ results in the following stady-state values for the dq-current components:

$$i_{1,d,0} = \frac{V_{1,0} \cdot \left(R_2 + \frac{4}{\pi} \frac{V_{dc,out,0}}{I_{2,0}} \right)}{R_1 \cdot R_2 + R_1 \cdot \frac{4}{\pi} \frac{V_{dc,out,0}}{I_{2,0}} + \omega_0^2 M^2} \approx \frac{4}{\pi} \cdot \frac{V_{dc,out,0}}{\omega_0 M} \tag{3.30a}$$

$$i_{2,q,0} = \frac{\omega_0 M \cdot V_{1,0} - R_1 \cdot \frac{4}{\pi} \cdot V_{dc,out,0}}{R_1 \cdot R_2 + \omega_0^2 M^2} \approx -\frac{V_{1,0}}{\omega_0 M} \tag{3.30b}$$

$$i_{1,q,0} = 0 \tag{3.30c}$$

$$i_{2,d,0} = 0 \tag{3.30d}$$

The approximation is done by ignoring the resistances, as these can be assumed very small.

Inserting these components into the steady-state equations of 3.26-3.29, the steady-

state solutions for the voltages is found to be:

$$0 = \omega_0 \cdot v_{C1,q,0} + \frac{1}{C_1} \cdot i_{1,d,0}$$
$$\Rightarrow v_{C1,q,0} = -\frac{1}{C_1\omega_0} \cdot i_{1,d,0} = -\frac{4}{\pi} \cdot \frac{V_{dc,out,0}}{C_1\omega_0^2 M} \tag{3.31a}$$

$$0 = -\omega_0 \cdot v_{C1,d,0} + \frac{1}{C_1} \cdot i_{1,q,0}$$
$$\Rightarrow v_{C1,d,0} = 0 \tag{3.31b}$$

$$0 = \omega_0 \cdot v_{C2,q,0} + \frac{1}{C_1} \cdot i_{2,d,0}$$
$$\Rightarrow v_{C2,q,0} = 0 \tag{3.31c}$$

$$0 = -\omega_0 \cdot v_{C2,d,0} + \frac{1}{C_1} \cdot i_{2,q,0}$$
$$\Rightarrow v_{C2,d,0} = \frac{1}{C_2\omega_0} \cdot i_{2,q,0} = -\frac{V_{1,0}}{C_2\omega_0^2 M} \tag{3.31d}$$

These steady-state solutions are only valid when assuming resonant frequency $\omega = \omega_0 = \frac{1}{\sqrt{L_1 C_1}} = \frac{1}{\sqrt{L_2 C_2}}$.

3.3 Small-signal IPT-model

The linearized model describing the small-signal dynamics can be written in compact form as:

$$\Delta\dot{\mathbf{x}} = \mathbf{A}(\mathbf{x}_0, \mathbf{u}_0) \cdot \Delta\mathbf{x} + \mathbf{B}(\mathbf{x}_0, \mathbf{u}_0) \cdot \Delta\mathbf{u} \tag{3.32}$$

where

$$\mathbf{A}(\mathbf{x}_0, \mathbf{u}_0) = \left.\frac{\partial f_i}{\partial \mathbf{x}}\right|_{\mathbf{x}_0,\mathbf{u}_0} \qquad \mathbf{B}(\mathbf{x}_0, \mathbf{u}_0) = \left.\frac{\partial f_i}{\partial \mathbf{u}}\right|_{\mathbf{x}_0,\mathbf{u}_0} \tag{3.33}$$

Expanding the formula of 3.33 in matrix form results in the following matrices of the linearized model:

$$\boldsymbol{A} = \begin{pmatrix} \frac{\partial f_1}{\partial x_1} & \frac{\partial f_1}{\partial x_2} & \frac{\partial f_1}{\partial x_3} & \frac{\partial f_1}{\partial x_4} & \frac{\partial f_1}{\partial x_5} & \frac{\partial f_1}{\partial x_6} & \frac{\partial f_1}{\partial x_7} & \frac{\partial f_1}{\partial x_8} \\ \frac{\partial f_2}{\partial x_1} & \frac{\partial f_2}{\partial x_2} & \frac{\partial f_2}{\partial x_3} & \frac{\partial f_2}{\partial x_4} & \frac{\partial f_2}{\partial x_5} & \frac{\partial f_2}{\partial x_6} & \frac{\partial f_2}{\partial x_7} & \frac{\partial f_2}{\partial x_8} \\ \frac{\partial f_3}{\partial x_1} & \frac{\partial f_3}{\partial x_2} & \frac{\partial f_3}{\partial x_3} & \frac{\partial f_3}{\partial x_4} & \frac{\partial f_3}{\partial x_5} & \frac{\partial f_3}{\partial x_6} & \frac{\partial f_3}{\partial x_7} & \frac{\partial f_3}{\partial x_8} \\ \frac{\partial f_4}{\partial x_1} & \frac{\partial f_4}{\partial x_2} & \frac{\partial f_4}{\partial x_3} & \frac{\partial f_4}{\partial x_4} & \frac{\partial f_4}{\partial x_5} & \frac{\partial f_4}{\partial x_6} & \frac{\partial f_4}{\partial x_7} & \frac{\partial f_4}{\partial x_8} \\ \frac{\partial f_5}{\partial x_1} & \frac{\partial f_5}{\partial x_2} & \frac{\partial f_5}{\partial x_3} & \frac{\partial f_5}{\partial x_4} & \frac{\partial f_5}{\partial x_5} & \frac{\partial f_5}{\partial x_6} & \frac{\partial f_5}{\partial x_7} & \frac{\partial f_5}{\partial x_8} \\ \frac{\partial f_6}{\partial x_1} & \frac{\partial f_6}{\partial x_2} & \frac{\partial f_6}{\partial x_3} & \frac{\partial f_6}{\partial x_4} & \frac{\partial f_6}{\partial x_5} & \frac{\partial f_6}{\partial x_6} & \frac{\partial f_6}{\partial x_7} & \frac{\partial f_6}{\partial x_8} \\ \frac{\partial f_7}{\partial x_1} & \frac{\partial f_7}{\partial x_2} & \frac{\partial f_7}{\partial x_3} & \frac{\partial f_7}{\partial x_4} & \frac{\partial f_7}{\partial x_5} & \frac{\partial f_7}{\partial x_6} & \frac{\partial f_7}{\partial x_7} & \frac{\partial f_7}{\partial x_8} \\ \frac{\partial f_8}{\partial x_1} & \frac{\partial f_8}{\partial x_2} & \frac{\partial f_8}{\partial x_3} & \frac{\partial f_8}{\partial x_4} & \frac{\partial f_8}{\partial x_5} & \frac{\partial f_8}{\partial x_6} & \frac{\partial f_7}{\partial x_7} & \frac{\partial f_8}{\partial x_8} \end{pmatrix} \Bigg|_{\boldsymbol{x_0}, \boldsymbol{u_0}} \tag{3.34}$$

$$\boldsymbol{B} = \begin{pmatrix} \frac{\partial f_1}{\partial u_1} & \frac{\partial f_1}{\partial u_2} & \frac{\partial f_1}{\partial u_3} & \frac{\partial f_1}{\partial u_4} \\ \frac{\partial f_2}{\partial u_1} & \frac{\partial f_2}{\partial u_2} & \frac{\partial f_2}{\partial u_3} & \frac{\partial f_2}{\partial u_4} \\ \frac{\partial f_3}{\partial u_1} & \frac{\partial f_3}{\partial u_2} & \frac{\partial f_3}{\partial u_3} & \frac{\partial f_3}{\partial u_4} \\ \frac{\partial f_4}{\partial u_1} & \frac{\partial f_4}{\partial u_2} & \frac{\partial f_4}{\partial u_3} & \frac{\partial f_4}{\partial u_4} \\ \frac{\partial f_5}{\partial u_1} & \frac{\partial f_5}{\partial u_2} & \frac{\partial f_5}{\partial u_3} & \frac{\partial f_5}{\partial u_4} \\ \frac{\partial f_6}{\partial u_1} & \frac{\partial f_6}{\partial u_2} & \frac{\partial f_6}{\partial u_3} & \frac{\partial f_6}{\partial u_4} \\ \frac{\partial f_7}{\partial u_1} & \frac{\partial f_7}{\partial u_2} & \frac{\partial f_7}{\partial u_3} & \frac{\partial f_7}{\partial u_4} \\ \frac{\partial f_8}{\partial u_1} & \frac{\partial f_8}{\partial u_2} & \frac{\partial f_8}{\partial u_3} & \frac{\partial f_8}{\partial u_4} \end{pmatrix} \Bigg|_{\boldsymbol{x_0}, \boldsymbol{u_0}} \tag{3.35}$$

Computing the elements of these matrices is quite uncomplicated, except a couple

of troublesome entries in the $\boldsymbol{A}$-matrix, namely:

$$\begin{aligned} A_{1,3} &= \frac{\partial f_1}{\partial i_{2,d}} = \frac{MR_2}{L_{\alpha 1}L_2} \\ &\quad + \frac{4}{\pi}\frac{MV_{dc,out}}{L_{\alpha 1}L_2}\left.\frac{\sqrt{i_{2,d}^2+i_{2,q}^2}-\frac{2i_{2,d}}{2\sqrt{i_{2,d}^2+i_{2,q}^2}}}{i_{2,d}^2+i_{2,q}^2}\right|_{i_{2,d}=0, i_{2,q}=-\frac{V_{1,0}}{\omega_0 M}} \\ &= \frac{MR_2}{L_{\alpha 1}L_2} + \frac{4}{\pi}\frac{MV_{dc,out}}{L_{\alpha 1}L_2}\frac{\omega_0 M}{V_{1,0}} = \frac{M\left(R_2 + \frac{4}{\pi}\frac{V_{dc,out}}{V_{1,0}}\cdot\omega_0 M\right)}{L_{\alpha 1}L_2} \end{aligned} \tag{3.36a}$$

$$\begin{aligned} A_{3,3} &= \frac{\partial f_3}{\partial i_{2,d}} = -\frac{R_2}{L_{\alpha 2}} \\ &\quad - \frac{4}{\pi}\frac{V_{dc,out}}{L_{\alpha 2}}\left.\frac{\sqrt{i_{2,d}^2+i_{2,q}^2}-\frac{2i_{2,d}}{2\sqrt{i_{2,d}^2+i_{2,q}^2}}}{i_{2,d}^2+i_{2,q}^2}\right|_{i_{2,d}=0, i_{2,q}=-\frac{V_{1,0}}{\omega_0 M}} \\ &= -\frac{R_2}{L_{\alpha 2}} - \frac{4}{\pi}\frac{V_{dc,out}}{L_{\alpha}2}\frac{\omega_0 M}{V_{1,0}} = -\frac{\left(R_2 + \frac{4}{\pi}\frac{V_{dc,out}}{V_{1,0}}\cdot\omega_0 M\right)}{L_{\alpha 2}} \end{aligned} \tag{3.36b}$$

All other elements can be easily found by straightforward derivation and insertion of the steady-state values. However, these calculations are not shown here due to the unnecessary use of space. By inserting the obtained results in matrix 3.34 and 3.35, the matrices are found to be:

$$\mathbf{A} = \begin{pmatrix} -\frac{R_1}{L_{\alpha1}} & \omega_0 & A_{1,3} & 0 & -\frac{1}{L_{\alpha1}} & 0 & \frac{M}{L_{\alpha1}L_2} & 0 \\ -\omega_0 & -\frac{R_1}{L_{\alpha1}} & 0 & \frac{MR_2}{L_{\alpha1}L_2} & 0 & -\frac{1}{L_{\alpha1}} & 0 & \frac{M}{L_{\alpha1}L_2} \\ \frac{MR_1}{L_{\alpha2}L_1} & 0 & A_{3,3} & \omega_0 & \frac{M}{L_{\alpha2}L_1} & 0 & -\frac{1}{L_{\alpha2}} & 0 \\ 0 & \frac{MR_1}{L_{\alpha2}L_1} & -\omega_0 & \frac{R_2}{L_{\alpha2}} & 0 & \frac{M}{L_{\alpha2}L_1} & 0 & -\frac{1}{L_{\alpha2}} \\ \frac{1}{C_1} & 0 & 0 & 0 & 0 & \omega_0 & 0 & 0 \\ 0 & \frac{1}{C_1} & 0 & 0 & -\omega_0 & 0 & 0 & 0 \\ 0 & 0 & \frac{1}{C_2} & 0 & 0 & 0 & 0 & \omega_0 \\ 0 & 0 & 0 & \frac{1}{C_2} & 0 & 0 & -\omega_0 & 0 \end{pmatrix} \tag{3.37}$$

$$\mathbf{B} = \begin{pmatrix} \frac{1}{L_{\alpha1}} & 0 & 0 & 0 \\ 0 & \frac{1}{L_{\alpha1}} & -i_{1,d,0} & -\frac{4}{\pi}\frac{M}{L_{\alpha1}L_2} \\ -\frac{M}{L_{\alpha2}L_1} & 0 & i_{2,q,0} & 0 \\ 0 & -\frac{M}{L_{\alpha2}L_1} & 0 & \frac{4}{\pi}\frac{1}{L_{\alpha2}} \\ 0 & 0 & v_{C1,q,0} & 0 \\ 0 & 0 & 0 & 0 \\ 0 & 0 & 0 & 0 \\ 0 & 0 & -v_{C2,d,0} & 0 \end{pmatrix} \tag{3.38}$$

Where $A_{1,3}$ and $A_{3,3}$ are the results found in equation 3.36a and 3.36b, respectively. Thus, the lineariezd model is described in state-space representation as:

$$\Delta\dot{\mathbf{x}} = \mathbf{A}(\mathbf{x}_0, \mathbf{u}_0) \cdot \Delta\mathbf{x} + \mathbf{B}(\mathbf{x}_0, \mathbf{u}_0) \cdot \Delta\mathbf{u} \tag{3.39}$$

where matrix $\boldsymbol{A}$ and $\boldsymbol{B}$ are reported in equation 3.37 and 3.38, respectively, and the state vector $\boldsymbol{x}$ and input vector $\boldsymbol{u}$ are as follows:

$$\Delta \boldsymbol{x} = \begin{bmatrix} \Delta i_{1,d} & \Delta i_{1,q} & \Delta i_{2,d} & \Delta i_{2,q} & \Delta v_{C1,d} & \Delta v_{C1,q} & \Delta v_{C2,d} & \Delta v_{C2,q} \end{bmatrix}^T \tag{3.40}$$

$$\Delta \boldsymbol{u} = \begin{bmatrix} \Delta v_{1,d} & \Delta v_{1,q} & \Delta \omega & \Delta V_{dc,out} \end{bmatrix}^T \tag{3.41}$$

where $\Delta \boldsymbol{x} = \boldsymbol{x} - \boldsymbol{x}_0$ and $\Delta \boldsymbol{u} = \boldsymbol{u} - \boldsymbol{u}_0$.

Chapter 4

Stability and Sensitivity Analysis

4.1 Parameter values

The parameters used in the analysis of the system are expressed in Table 4.1.

Table 4.1: PARAMETERS OF ANALYZED IPT-SYSTEM

Nominal power, P_0	$10\ kW$
Nominal operating frequency, f_0	$85\ kHz$
Nominal coupling factor, k	0.2
Primary coil	
Nominal voltage, V_1	$380\ V$
Self-inductance, L_1	$176\ \mu F$
Quality factor, Q_1	310
Secondary coil	
Nominal voltage, V_2	$235\ V$
Self-inductance, L_2	$41\ \mu F$
Quality factor, Q_2	270

It is assumed that the transmitter and the receiver is tuned for the same resonance frequency f_0:

$$\omega_0 = \frac{1}{\sqrt{C_1 L_1}} = \frac{1}{\sqrt{C_2 L_2}} = 2\pi \cdot f_0 = 5.3407 \cdot 10^5 \text{ rad/s} \tag{4.1}$$

where ω_0 is the angular frequency of the power source. Thus, the capacitance on both sending and pickup side is to be found:

$$C_1 = \frac{1}{\omega_0^2 \cdot L_1} = \frac{1}{(2\pi \cdot 85000)^2 \cdot 176 \cdot 10^{-6}} = 0.01992 \ \mu\text{F} \tag{4.2a}$$

$$C_2 = \frac{1}{\omega_0^2 \cdot L_2} = \frac{1}{(2\pi \cdot 85000)^2 \cdot 41 \cdot 10^{-6}} = 0.08551 \ \mu\text{F} \tag{4.2b}$$

The measure of an inductor's efficiency, the quality factor, is the ratio between the inductive reactance and resistance at a given frequency, namely:

$$Q = \frac{\omega L}{R} \tag{4.3}$$

Thus the resistance in both coils can be computed:

$$R_1 = \frac{\omega_0 \cdot L_1}{Q_1} = \frac{2\pi \cdot 85000 \cdot 176 \cdot 10^{-6}}{310} = 0.3032 \ \Omega \tag{4.4a}$$

$$R_2 = \frac{\omega_0 \cdot L_2}{Q_2} = \frac{2\pi \cdot 8500041 \cdot 10^{-6}}{270} = 0.0811 \ \Omega \tag{4.4b}$$

The coupling factor between the two coils is given by:

$$k = \frac{M}{\sqrt{L_1 L_2}} \tag{4.5}$$

and the mutual inductance is found as:

$$M = k \cdot \sqrt{L_1 L_2} = 0.2 \cdot \sqrt{176 \cdot 41 \cdot 10^{-12}} = 16.9894 \ \mu\text{F} \tag{4.6}$$

The leakage factor defined in 3.5 are computed as:

$$L_{\alpha 1} = L_1 - \frac{M^2}{L_2} = 176 \cdot 10^{-6} - \frac{(7.6452 \cdot 10^{-5})^2}{41 \cdot 10^{-6}} = 168.9600\ \mu\text{F} \tag{4.7a}$$

$$L_{\alpha 2} = L_2 - \frac{M^2}{L_1} = 41 \cdot 10^{-6} - \frac{(7.6452 \cdot 10^{-5})^2}{176 \cdot 10^{-6}} = 39.3600\ \mu\text{F} \tag{4.7b}$$

4.2 Eigenvalues and eigenvalue trajectory

Eigenvalues of the $\boldsymbol{A}$-matrix in the linearized model can be used to conduct stability analysis. This analysis describes the small signal behavior of the system, that is, the behavior of the system when linearized at the operating point $\boldsymbol{f}(\boldsymbol{x}, \boldsymbol{u}) = 0$. Plotting an eigenvalue in the complex plane by varying one or more parameters of the $\boldsymbol{A}$-matrix is called an eigenvalue trajectory. A stable system has all the eigenvalues located at the left-hand side of the imaginary axis in the complex plane. The eigenvalues located closer to the imaginary axis are the critical mode of the system; those eigenvalues dominate the others and are the least damped modes. If any eigenvalues were located in the right half plane, it would render the system unstable. Thus, a stability analysis could be conducted by looking at the trajectory of the eigenvalues while varying known dynamic parameters of the model.

The eigenvalues of matrix 3.34 with the nominal numerical values inserted is:

$$eig(\boldsymbol{A}) = \begin{bmatrix} -2.2161 \cdot 10^4 \pm i1.1266 \cdot 10^6 \\ -1.5247 \cdot 10^4 \pm i1.0232 \cdot 10^6 \\ -2.9488 \cdot 10^3 \pm i5.3551 \cdot 10^4 \\ -3.4780 \cdot 10^4 \pm i4.3116 \cdot 10^4 \end{bmatrix} \tag{4.8}$$

4.2.1 Varying the load voltage

As the load may differ during operation of the system, it is of great interest to see how the eigenvalues change with varying load.

The trajectories of the eigenvalues of the $\boldsymbol{A}$-matrix when the load voltage are varied in the range $0.5V_{2,nom} \leq V_2 \leq 2V_{2,nom}$ and all other parameters are kept constant is depicted in Figure 4.1.

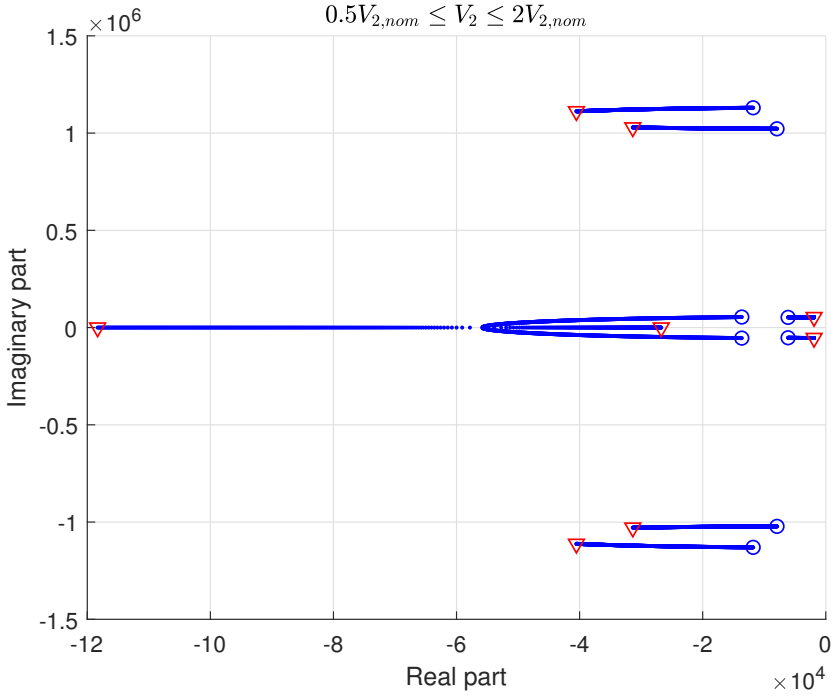

Figure 4.1: Eigenvalue trajectories when the load voltage is varied. Blue circle is the lowest load, whereas red triangle is the highest load.

From Figure 4.1 it is clear that the critical modes of the system are the rightmost pole pair. Moreover, it is easy to see that the pole pair approaches the imaginary axis when the load increases, thus lowering the damping and increasing the settling time of the mode.

4.2.2 Varying the coupling coefficient

As the magnetic coupling may differ during operation of the system, it is also of great interest to observe how the eigenvalues change with varying coupling.

The trajectories of the eigenvalues of the $\boldsymbol{A}$-matrix when the magnetic coupling are varied in the range $0.5k_{nom} \leq k \leq 2k_{nom}$ and all other parameters are kept constant is shown in Figure 4.2.

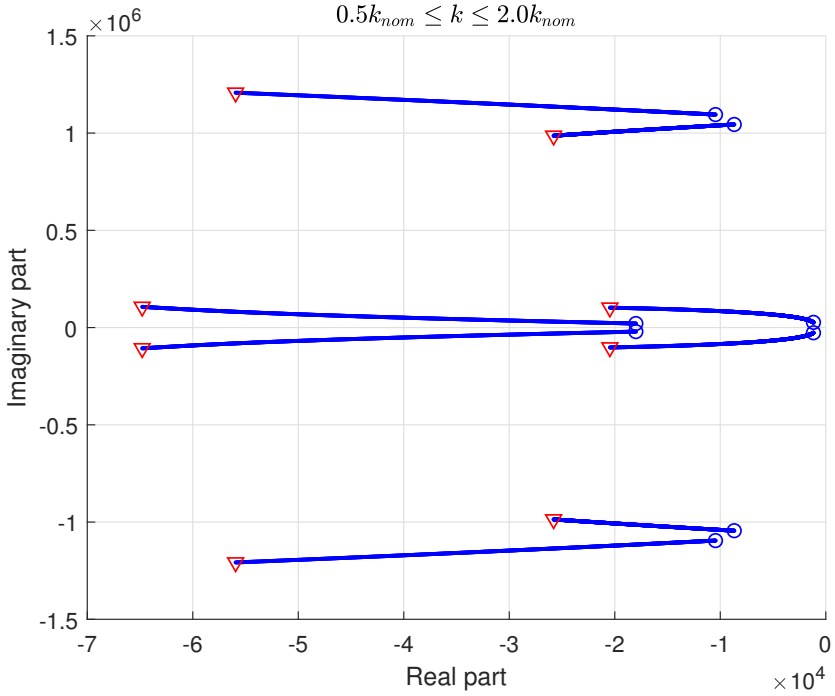

Figure 4.2: Eigenvalue trajectories when the coupling coefficient is varied. Blue circle is the lowest load, whereas red triangle is the highest load.

The same problem modes can be observed in Figure 4.2 as well. It can easily be seen that the real part of the critical pole pair rapidly decreases in absolute value when the magnetic coupling decreases and consequently lowering the damping and increasing the settling time of the mode.

4.3 Participation factors

According to 4.8, the eigenvalues of the $\boldsymbol{A}$-matrix in 3.33 of the linearized model 3.32 simulated with the parameters listed in Table 4.1 are all complex conjugate pairs. To handle this matter, the first method has been adjusted to include the absolute values of the participation factors. Four methods of calculation the participation factors have been explored:

Method I:

$$p_{ki} = |l_k^i r_k^i| \tag{4.9}$$

Method II:

$$p_{ki} = \frac{(\Re\{l_k^i\})^2}{\Re\{l^i\}(\Re\{l^i\})^T} \tag{4.10}$$

Method III:

$$p_{ki} = \frac{|l_k^i|^2}{\sum_{j=1}^{n} |l_j^i|} \tag{4.11}$$

Method IV:

$$p_{ki} = 2\Re\{l_k^i r_k^i\}) \tag{4.12}$$

The respective results are shown in Table 4.2, 4.3, 4.4 and 4.5.

Table 4.2: PARTICIPATION FACTORS METHOD I

State	Mode 1	Mode 2	Mode 3	Mode 4
$i_{1,d}$	0.1323	0.1308	0.2660	0.0170
$i_{1,q}$	0.1334	0.1319	0.0202	0.3449
$i_{2,d}$	0.1322	0.1332	0.0217	0.3526
$i_{2,q}$	0.1321	0.1336	0.2595	0.0107
$v_{C1,d}$	0.1325	0.1310	0.0173	0.3441
$v_{C1,q}$	0.1332	0.1316	0.2633	0.0138
$v_{C2,d}$	0.1318	0.1332	0.2741	0.0282
$v_{C2,q}$	0.1323	0.1337	0.0195	0.3457

The critical mode of the system observed and discussed in Section 4.2 is labelled as Mode 3. It can be observed that the states which participates most in the problem mode according to this method is $i_{1,d}$, $i_{2,q}$, $v_{C1,q}$ and $v_{C2,d}$. The reason may

be that $i_{1,d}$ and $i_{2,q}$ are the states that determines the steady-state power flow of the system, and that $v_{C1,q}$ and $v_{C2,d}$ are connected to $i_{1,d}$ and $i_{2,q}$ through the general formulae $v_c(s) = \frac{-j\omega}{C} i_c(s)$. That is, the voltage is phase shifted by 90 degrees and it is therefore a direct connection between the q-axis capacitor voltage and d-axis current, and vica versa.

Mode 4 of this table are the most damped eigenvalues, and it can be seen that the set of states which participates most in this mode are the complement of the set of states that participates most in the critical mode. These states probably have the least effect on the overall model response and dynamics of interest. Mode 1 and 2 are the most oscillating modes and all the states participate almost equally in these, which are probably describing the LC-oscillations of the circuit.

Table 4.3: PARTICIPATION FACTORS METHOD II

State	Mode 1	Mode 2	Mode 3	Mode 4
$i_{1,d}$	0.6480	0.6899	0.9544	0.0356
$i_{1,q}$	0.1675	0.1202	0.1202	0.9596
$i_{2,d}$	0.1838	0.1893	0.0100	$1.3252 \cdot 10^{-4}$
$i_{2,q}$	$6.7051 \cdot 10^{-5}$	$1.7255 \cdot 10^{-5}$	$1.5038 \cdot 10^{-5}$	0.0045
$v_{C1,d}$	$1.8746 \cdot 10^{-5}$	$1.3158 \cdot 10^{-5}$	$4.0442 \cdot 10^{-6}$	$1.0868 \cdot 10^{-4}$
$v_{C1,q}$	$9.3431 \cdot 10^{-5}$	$6.3781 \cdot 10^{-5}$	$1.0673 \cdot 10^{-4}$	$4.1201 \cdot 10^{-6}$
$v_{C2,d}$	$2.9534 \cdot 10^{-7}$	$2.7875 \cdot 10^{-8}$	$8.5123 \cdot 10^{-8}$	$9.0091 \cdot 10^{-7}$
$v_{C2,q}$	$4.7722 \cdot 10^{-4}$	$3.4115 \cdot 10^{-4}$	$6.0590 \cdot 10^{-6}$	$8.6470 \cdot 10^{-8}$

Table 4.4: PARTICIPATION FACTORS METHOD III

State	Mode 1	Mode 2	Mode 3	Mode 4
$i_{1,d}$	0.4055	0.4033	0.7813	0.0272
$i_{1,q}$	0.4068	0.4041	0.0316	0.7804
$i_{2,d}$	0.0942	0.0963	0.0144	0.1906
$i_{2,q}$	0.0929	0.0958	0.1722	0.0013
$v_{C1,d}$	$5.5935 \cdot 10^{-5}$	$3.8426 \cdot 10^{-5}$	$3.4773 \cdot 10^{-6}$	$9.1180 \cdot 10^{-5}$
$v_{C1,q}$	$5.6409 \cdot 10^{-5}$	$3.8704 \cdot 10^{-5}$	$8.7375 \cdot 10^{-5}$	$1.3561 \cdot 10^{-6}$
$v_{C2,d}$	$2.3766 \cdot 10^{-4}$	$1.6955 \cdot 10^{-4}$	$3.9006 \cdot 10^{-4}$	$2.1957 \cdot 10^{-5}$
$v_{C2,q}$	$2.3918 \cdot 10^{-4}$	$1.7068 \cdot 10^{-4}$	$1.7983 \cdot 10^{-5}$	$3.9207 \cdot 10^{-4}$

These two above methods seem to emphasize that the states describing the voltages are defined by the integral av the currents, i.e. that they do not give any additional information on the system. These tables are mostly displayed for comparison purposes and are not further analyzed.

Table 4.5: PARTICIPATION FACTORS METHOD IV

State	Mode 1	Mode 2	Mode 3	Mode 4
$i_{1,d}$	0.240	0.2508	0.5316	0.0017
$i_{1,q}$	0.2458	0.2544	0.0296	0.5460
$i_{2,d}$	0.2558	0.2469	0.0339	0.5630
$i_{2,q}$	0.2543	0.2455	0.5188	0.0047
$v_{C1,d}$	0.2502	0.2474	0.0347	0.5328
$v_{C1,q}$	0.2515	0.2485	0.5266	0.0213
$v_{C2,d}$	0.2488	0.2514	0.5481	0.0437
$v_{C2,q}$	0.2498	0.2525	0.0390	0.5353

This fourth method gives the same information as the first method, and the same conclusion can be drawn.

Chapter 5

Gramians and Transfer Functions

5.1 Analysis of the controllability Gramian

As described in the theory chapter, there are several ways of measuring and interpret the degree of controllability by analyzing the controllability Gramian:

1) $tr(\boldsymbol{W}_c)$
2) $det(\boldsymbol{W}_c)$
3) $\lambda_{min}(\boldsymbol{W}_c)$
4) $eigenvectors$
5) $rank(\boldsymbol{W}_c)$

The state-space model in 3.39 is described by eight state variables and four input variables. However, it is possible to have several different input configurations, e.g. one where the input voltages on both sending and receiving side are controlled, one where only the input voltage on the sending side is controlled and one where only the input voltage on the receiving side is controlled. Moreover, by assuming the resonant frequency w_0 to be constant throughout the operation of the system, this input variable could in that particular case be treated as a parameter. In addition, by considering the synchronization of the dq-reference frame, $v_{1,q} = 0$ in steady-state and this input variable could therefore, in that case, be neglected. These assumptions and modifications result in several different variants

of the $\boldsymbol{B}$-matrix in the linearized model.

5.1.1 Considering all input variables

This section considers both ω and $v_{1,q}$.

1) Input voltages on both sending and receiving side

This is the base configuration and no changes are made. The input vector $\boldsymbol{u}$ and matrix $\boldsymbol{B}$ are the same as displayed in equation 3.41 and 3.38, respectively. Computing the smallest eigenvalue of the controllability Gramian with both sending and receiving voltage as input gives the following result:

$$\lambda_{min}(\boldsymbol{W}_c) = 251.4753 \tag{5.1}$$

The eigenvector corresponding to this eigenvalue is:

$$\boldsymbol{\xi} = \begin{bmatrix} -0.2017 \\ 0.8452 \\ -0.4943 \\ 0.0028 \\ 0..0072 \\ 2.2857 \cdot 10^{-4} \\ -0.0059 \\ 0.0224 \end{bmatrix} \tag{5.2}$$

Thus, this is the direction in the state-space which is hardest to control. The trace of the Gramian, which describes the average controllability in all of the directions in the state-space, is found to be:

$$tr(\boldsymbol{W}_c) = 8.3450 \cdot 10^7 \tag{5.3}$$

and the volume enclosed by the ellipsis defined by $\boldsymbol{W}_c$ is calculated, using the determinant, as:

$$V(\mathcal{E}_{min}) = 1.3813 \cdot 10^3 \tag{5.4}$$

2) Input voltage on only the sending side

This configuration reduces the input vector $\boldsymbol{u}$ and matrix $\boldsymbol{B}$ to:

$$\boldsymbol{u} = \begin{bmatrix} v_{1,d} \\ v_{1_q} \\ \omega \end{bmatrix} \quad \boldsymbol{B} = \begin{pmatrix} \frac{1}{L_{\alpha 1}} & 0 & 0 \\ 0 & \frac{1}{L_{\alpha 1}} & -i_{1,d,0} \\ -\frac{M}{L_{\alpha 2} L_1} & 0 & i_{2,q,0} \\ 0 & -\frac{M}{L_{\alpha 2} L_1} & \\ 0 & 0 & v_{C1,q,0} \\ 0 & 0 & 0 \\ 0 & 0 & 0 \\ 0 & 0 & -v_{C2,d,0} \end{pmatrix} \tag{5.5}$$

Now the smallest eigenvalue of the controllability Gramian is:

$$\lambda_{min}(\boldsymbol{W}_c) = 134.2109 \tag{5.6}$$

and the corresponding eigenvector:

$$\boldsymbol{\xi} = \begin{bmatrix} 0.3180 \\ -0.8488 \\ 0.4155 \\ -0.0723 \\ -0.0046 \\ 0.0012 \\ 0.0081 \\ -0.0214 \end{bmatrix} \tag{5.7}$$

The trace of the Gramian and volume of the ellipsis is:

$$tr(\boldsymbol{W}_c) = 1.4012 \cdot 10^7 \tag{5.8a}$$

$$V(\mathcal{E}_{min}) = 703.3867 \tag{5.8b}$$

3) Input voltage on only the receiving side

This configuration reduces the input vector $\boldsymbol{u}$ and matrix $\boldsymbol{B}$ to:

$$\boldsymbol{u} = \begin{bmatrix} \omega \\ V_{dc,out} \end{bmatrix} \quad \boldsymbol{B} = \begin{pmatrix} 0 & 0 \\ -i_{1,d,0} & -\frac{4}{\pi}\frac{M}{L_{\alpha 1}L_2} \\ i_{2,q,0} & 0 \\ 0 & \frac{4}{\pi}\frac{1}{L_{\alpha 2}} \\ v_{C1,q,0} & 0 \\ 0 & 0 \\ 0 & 0 \\ -v_{C2,d,0} & 0 \end{pmatrix} \tag{5.9}$$

Here, the smallest eigenvalue is:

$$\lambda_{min}(\boldsymbol{W}_c) = 75.5097 \tag{5.10}$$

with the corresponding eigenvector:

$$\boldsymbol{\xi} = \begin{bmatrix} 0.2075 \\ -0.9716 \\ 0.0963 \\ -0.0589 \\ -0.0094 \\ 0.0018 \\ 2.0853 \cdot 10^{-4} \\ -0..0044 \end{bmatrix} \tag{5.11}$$

The trace of the Gramian and volume of the ellipsis is:

$$tr(\boldsymbol{W}_c) = 6.9438 \cdot 10^7 \tag{5.12a}$$
$$V(\mathcal{E}_{min}) = 1.0148 \cdot 10^3 \tag{5.12b}$$

5.1.2 Neglecting the q-axis input voltage

Now, $v_{1,q}$ are considered to be zero, thus removed from the input vector $\boldsymbol{u}$, and the corresponding column in the $\boldsymbol{B}$-matrix is eliminated.

1) Input voltages on both sending and receiving side

Elimination of $v_{1,q}$ results in the following input vector $\boldsymbol{u}$ and $\boldsymbol{B}$-matrix:

$$\boldsymbol{u} = \begin{bmatrix} v_{1,d} \\ \omega \\ V_{dc,out} \end{bmatrix} \quad \boldsymbol{B} = \begin{pmatrix} \frac{1}{L_{\alpha 1}} & 0 & 0 \\ 0 & -i_{1,d,0} & -\frac{4}{\pi}\frac{M}{L_{\alpha 1}L_2} \\ -\frac{M}{L_{\alpha 2}L_1} & i_{2,q,0} & \\ 0 & 0 & \frac{4}{\pi}\frac{1}{L_{\alpha 2}} \\ 0 & v_{C1,q,0} & 0 \\ 0 & 0 & 0 \\ 0 & 0 & 0 \\ 0 & -v_{C2,d,0} & 0 \end{pmatrix} \tag{5.13}$$

The smallest eigenvalue is found to be:

$$\lambda_{min}(\boldsymbol{W}_c) = 79.9368 \tag{5.14}$$

The eigenvector corresponding to this eigenvalue is:

$$\boldsymbol{\xi} = \begin{bmatrix} -0.1596 \\ 0.9214 \\ -0.3519 \\ 0.0362 \\ 0.0094 \\ 8.3344 \cdot 10^{-4} \\ -0.0033 \\ 0.0165 \end{bmatrix} \tag{5.15}$$

The trace of the Gramian and volume of the ellipsis is:

$$tr(\boldsymbol{W}_c) = 7.9773 \cdot 10^7 \tag{5.16a}$$
$$V(\mathcal{E}_{min}) = 1.1068 \cdot 10^3 \tag{5.16b}$$

2) Input voltage on only the sending side

This configuration reduces the input vector $\boldsymbol{u}$ and matrix $\boldsymbol{B}$ to:

$$\boldsymbol{u} = \begin{bmatrix} v_{1,d} \\ \omega \end{bmatrix} \quad \boldsymbol{B} = \begin{pmatrix} \frac{1}{L_{\alpha 1}} & 0 \\ 0 & -i_{1,d,0} \\ -\frac{M}{L_{\alpha 2} L_1} & i_{2,q,0} \\ 0 & 0 \\ 0 & v_{C1,q,0} \\ 0 & 0 \\ 0 & 0 \\ 0 & -v_{C2,d,0} \end{pmatrix} \tag{5.17}$$

Now the smallest eigenvalue of the controllability Gramian is:

$$\lambda_{min}(\boldsymbol{W}_c) = 2.2953 \tag{5.18}$$

and the corresponding eigenvector:

$$\boldsymbol{\xi} = \begin{bmatrix} -0.1708 \\ 0.9234 \\ -0.3416 \\ 0.0332 \\ 0.0100 \\ 0.0011 \\ -0.0031 \\ 0.0153 \end{bmatrix} \tag{5.19}$$

The trace of the Gramian and volume of the ellipsis is:

$$tr(\boldsymbol{W}_c) = 1.0335 \cdot 10^7 \tag{5.20a}$$

$$V(\mathcal{E}_{min}) = 374.6536 \tag{5.20b}$$

3) Input voltage on only the receiving side

This configuration gives the same results as obtained in the corresponding case above. Therefore, the reduced input vector $\boldsymbol{u}$ and matrix $\boldsymbol{B}$ are omitted. The main results are, however, repeated for comparison purposes:

$$\lambda_{min}(\boldsymbol{W}_c) = 75.5097 \tag{5.21a}$$

$$tr(\boldsymbol{W}_c) = 6.9438 \cdot 10^7 \tag{5.21b}$$

$$V(\mathcal{E}_{min}) = 1.0148 \cdot 10^3 \tag{5.21c}$$

$$\boldsymbol{\xi} = \begin{bmatrix} 0.1547 \\ -0.8998 \\ 0.4062 \\ -0.0301 \\ -0.0092 \\ -6.4202 \cdot 10^{-4} \\ 0.0040 \\ -0.0190 \end{bmatrix} \tag{5.22}$$

5.1.3 Assuming the frequency as a constant

Six different cases arise with this condition as well. In the following, the calculations are done with the same configurations as above, i.e. with input voltages on both side, only on the sending side and only on the receiving side, both considering and neglecting. $v_{1,q}$ The resulting input vectors $\boldsymbol{u}$ and $\boldsymbol{B}$-matrices are omitted to avoid unnecessary use of space. The only differences from above are the elimination of ω_0 and the column of the $\boldsymbol{B}$-matrix corresponding to it. The case with only having control of the receiving side will be equal for both, but the results are repeated nonetheless.

1) Considering the q-axis input voltage

In the same order as above, the Gramian measures are found to be:

1) Input on both sides:

$$\lambda_{min}(\boldsymbol{W}_c) = 251.4676 \tag{5.23a}$$
$$tr(\boldsymbol{W}_c) = 8.3450 \cdot 10^7 \tag{5.23b}$$
$$V(\mathcal{E}_{min}) = 1.1813 \cdot 10^3 \tag{5.23c}$$

2) Input on only sending side:

$$\lambda_{min}(\boldsymbol{W}_c) = 134.2043 \tag{5.24a}$$
$$tr(\boldsymbol{W}_c) = 1.4012 \cdot 10^7 \tag{5.24b}$$
$$V(\mathcal{E}_{min}) = 703.3792 \tag{5.24c}$$

3) Input on only receiving side:

$$\lambda_{min}(\boldsymbol{W}_c) = 73.4969 \tag{5.25a}$$
$$tr(\boldsymbol{W}_c) = 6.9438 \cdot 10^7 \tag{5.25b}$$
$$V(\mathcal{E}_{min}) = 1.0147 \cdot 10^3 \tag{5.25c}$$

2) Neglecting the q-axis input voltage

Similarly:

1) Input on both sides:

$$\lambda_{min}(\boldsymbol{W}_c) = 79.9300 \tag{5.26a}$$
$$tr(\boldsymbol{W}_c) = 7.9773 \cdot 10^7 \tag{5.26b}$$
$$V(\mathcal{E}_{min}) = 1.1067 \cdot 10^3 \tag{5.26c}$$

2) Input on only sending side:

$$\lambda_{min}(\boldsymbol{W}_c) = 2.2915 \tag{5.27a}$$
$$tr(\boldsymbol{W}_c) = 1.0335 \cdot 10^7 \tag{5.27b}$$
$$V(\mathcal{E}_{min}) = 374.5748 \tag{5.27c}$$

3) Input on only receiving side:

$$\lambda_{min}(\boldsymbol{W}_c) = 73.4969 \tag{5.28a}$$
$$tr(\boldsymbol{W}_c) = 6.9438 \cdot 10^7 \tag{5.28b}$$
$$V(\mathcal{E}_{min}) = 1.0147 \cdot 10^3 \tag{5.28c}$$

.

The eigenvectors in all six cases are, respectively:

$$\boldsymbol{\xi}_{1,1} = \begin{bmatrix} -0.2017 \\ 0.8452 \\ -0.4943 \\ -0.0028 \\ 0.0072 \\ 2.2853 \cdot 10^{-4} \\ -0.0059 \\ 0.0224 \end{bmatrix} \quad \boldsymbol{\xi}_{2,1} = \begin{bmatrix} 0.3180 \\ -0.8488 \\ 0.4156 \\ -0.0732 \\ -0.0046 \\ 0.0012 \\ 0.0081 \\ -0.0214 \end{bmatrix} \quad \boldsymbol{\xi}_{3,1} = \begin{bmatrix} 0.2008 \\ -0.8406 \\ 0.5024 \\ 0.0042 \\ -0.0069 \\ -1.1477 \cdot 10^{-4} \\ 0.0059 \\ -0.0225 \end{bmatrix} \tag{5.29}$$

$$\boldsymbol{\xi}_{1,2} = \begin{bmatrix} 0.2055 \\ -0.9565 \\ 0.2023 \\ -0.0413 \\ -0.0094 \\ -0.0016 \\ 0.0017 \\ -0.0094 \end{bmatrix} \quad \boldsymbol{\xi}_{2,2} = \begin{bmatrix} -0.2130 \\ 0.9146 \\ -0.3430 \\ 0.0122 \\ 0.0099 \\ 0.0015 \\ -0.0036 \\ 0.0153 \end{bmatrix} \quad \boldsymbol{\xi}_{3,2} = \begin{bmatrix} 0.2075 \\ -0.9717 \\ 0.0960 \\ -0.0590 \\ -0.0094 \\ -0.0018 \\ 2.0424 \cdot 10^{-4} \\ -0.0044 \end{bmatrix} \tag{5.30}$$

In every case presented above, the controllable subspace is full, i.e. $rank(\boldsymbol{W}_c) = n$.

5.1.4 Summary of controllability Gramian measures

Table 5.1: SUMMARY OF CONTROLLABILITY GRAMIAN MEASURES

Base input	Possibilities	$\lambda_{min}(\boldsymbol{W}_c)$	$tr(\boldsymbol{W}_c)$	$V(\mathcal{E}_{min})$
Considering ω and $v_{1,q}$	1) Both	251.4753	$8.3450 \cdot 10^7$	$1.3813 \cdot 10^3$
	2) Sending	134.2109	$1.4012 \cdot 10^7$	703.3867
	3) Receiving	75.5097	$6.9438 \cdot 10^7$	$1.0148 \cdot 10^3$
Neglecting $v_{1,q}$	1) Both	79.9368	$7.9773 \cdot 10^7$	$1.0168 \cdot 10^3$
	2) Sending	2.2953	$1.0335 \cdot 10^7$	374.6536
	3) Receiving	75.5097	$6.9438 \cdot 10^7$	$1.0148 \cdot 10^3$
Neglecting ω, considering $v_{1,q}$	1) Both	251.4676	$8.3450 \cdot 10^7$	$1.1813 \cdot 10^3$
	2) Sending	134.2043	$1.4012 \cdot 10^7$	703.3792
	3) Receiving	73.4969	$6.9438 \cdot 10^7$	$1.0147 \cdot 10^3$
Neglecting ω and $v_{1,q}$	1) Both	79.9300	$7.9773 \cdot 10^7$	$1.1067 \cdot 10^3$
	2) Sending	2.2915	$1.0335 \cdot 10^7$	374.5748
	3) Receiving	73.4969	$6.9438 \cdot 10^7$	$1.0147 \cdot 10^3$

From Table 5.1, best controllability is achieved in every case when having the possibility of controlling the voltages on both sides. However, an interesting result arises in the case where both ω and $v_{1,q}$ are considered. It can be observed that the smallest eigenvalue is obtained when eliminating the control on the sending side, which means that it gets harder to control the system in a particular direction in the state-space. The average controllability, the trace of the Gramian, is however higher for the very same case, meaning that it is on average easier to control the whole system around in the state-space.

In the case where $v_{1,q}$ is neglected, a severe drop in controllability is obtained. It can also be observed that eliminating the possibility of actuating on the receiving side significantly decreases the controllability. The smallest eigenvalue is reduced

by a factor of approximately 35, and both trace and ellipsoid-volume are subject to notable decrease. However, reviving the possibility of actuating on the receiving side and at the same time eliminating the input control on the sending side give rise to a significant increase in all controllability measures compared to the case with an input signal only on the sending side. Compared to the case with the possibility of controlling the voltage on both sides, it can be seen that the controllability measures is not reduced by very much, meaning that having control on the receiving side is the main contributor to overall controllability in this particular case.

In the case where ω is treated as a parameter and thereby eliminated, it could be seen, by comparing the obtained measures with the corresponding results where ω is considered, that there is only a minor difference. In fact, the average controllability, i.e. the trace of the Gramian, in all cases seem identical with the corresponding results where the frequency input variable is considered. This is, however, due to the use of a precision of five significant figures. Using a precision of six significant figures or more, a slightly higher average controllability in the cases with ω as an input variable is visible. This could more easily be seen by investigating the trace of the inverse Gramian, which relates to the average energy needed to steer the system around in the state space, as this measure appears somewhat more sensitive to perturbations. The following only displays the trace of the inverse Gramian for the case without $v_{1,q}$. The same conclusion can, however, be drawn for the other case as well:

1) Input on both sides with and without ω_0, respectively:

$$tr(\boldsymbol{W}_{c,1}^{-1}) = 0.0169 \tag{5.31a}$$

$$tr(\boldsymbol{W}_{c,2}^{-1}) = 0.0170 \tag{5.31b}$$

2) Input on sending side with and without ω_0, respectively:

$$tr(\boldsymbol{W}_{c,1}^{-1}) = 0.4554 \tag{5.32a}$$

$$tr(\boldsymbol{W}_{c,2}^{-1}) = 0.4561 \tag{5.32b}$$

3) Input on receiving side with and without ω_0, respectively:

$$tr(\boldsymbol{W}_{c,1}^{-1}) = 0.0200 \tag{5.33a}$$

$$tr(\boldsymbol{W}_{c,2}^{-1}) = 0.0201 \tag{5.33b}$$

From this, it is evident that slightly more energy is needed to move the system around in the state-space without ω as an input variable. However, the differences are minor and show that the frequency input variable does not contribute a lot to overall controllability.

By looking at the vector defining the least controllable directions in the above sections, the eigenvectors, it can be noted that the absolute values of the entries, in general, do not differ much. However, some eigenvectors point in the opposite direction compared to the others. i.e. every entry has changed sign. This is no surprise since the energy ellipsoid defining the surface of how far in any direction it is possible to steer the system is symmetric about all axes. Thus, the opposite direction of the eigenvectors will always be just as little controllable as the direction of the eigenvector itself. Since the eigenvectors are quite similar, it means that the least controllable direction does not change much for the different cases.

5.2 Eigenvalue trajectory of the controllability Gramian

Every Gramian measures above is obtained with the nominal parameter values reported in Table 4.1. It is however of great interest to observe how the eigenvalues change when dynamic parameters of the system vary.

5.2.1 Varying the load voltage

The trajectories of the eigenvalues of the controllability Gramian when the load voltage is varied in the range $0.5V_{2,nom} \leq V_2 \leq 2V_{2,nom}$ and all other parameters are kept constant is depicted in Figure 5.1.

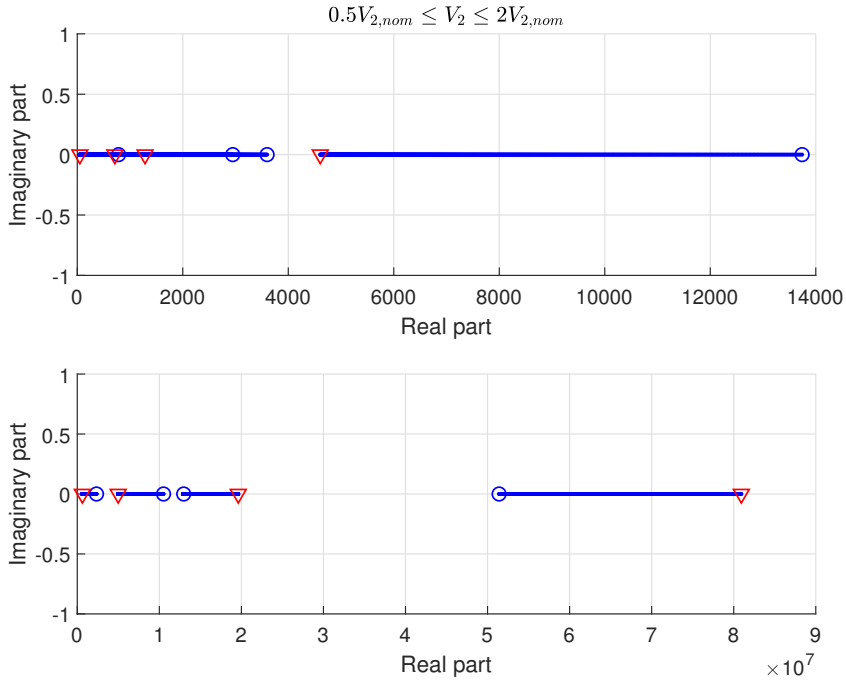

Figure 5.1: Eigenvalue trajectories of Gramian when the load voltage is varied. Blue circle is the lowest load, whereas red triangle is the highest load.

Since the eigenvalues of the Gramian always are real by definition, the eigenvalue trajectories are divided into two groups to avoid badly interpretable MATLAB plots. The uppermost figure displays the four smallest eigenvalues, whereas the lowermost figure displays the four largest eigenvalues. Clearly, the magnitude of the smallest eigenvalues decreases with increasing voltage load, meaning that the least controllable directions get even harder to control. The two largest eigenvalues, however, increases with increasing load, which means that the most controllable directions get easier to control.

It could also be of interest to observe how the average controllability, i.e. the trace of the Gramian, changes with varying load conditions. This is depicted in Figure 5.2

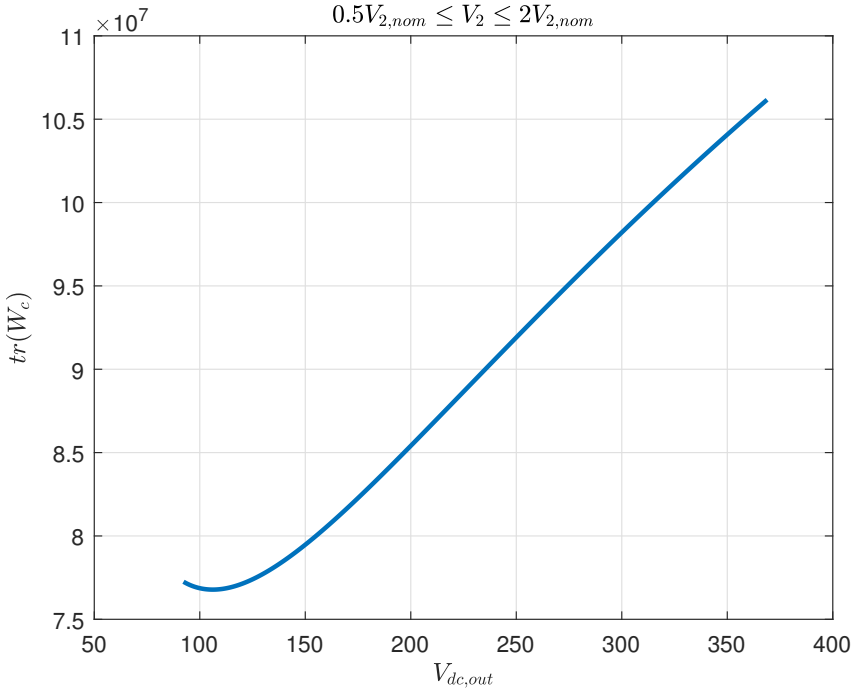

Figure 5.2: Trace of the Gramian with varying load voltage.

The trace of the Gramian increases with increasing load voltage, which means that the system, on average, gets easier to control. This seems contradictory to what was observed when considering the smallest eigenvalue trajectories. However, the two largest eigenvalues increase more than the smallest eigenvalues decreases when the load voltage is increased, thus producing the observed trace curve.

5.2.2 Varying the coupling coefficient

The trajectories of the eigenvalues of the controllability Gramian when the coupling coefficient is varied in the range $0.5k_{nom} \leq k \leq 2k_{nom}$ and all other parameters are kept constant is depicted in Figure 5.3.

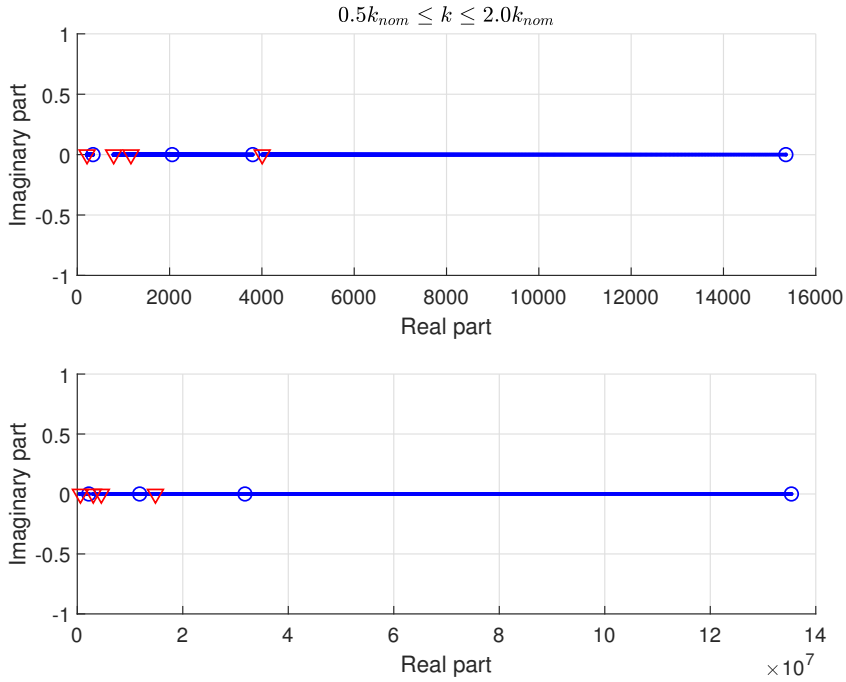

Figure 5.3: Eigenvalue trajectories of controllability Gramian when the coupling coefficient is varied. Blue circle is the lowest load, whereas red triangle is the highest load.

As for the trajectories with varying load, the uppermost figure is the four smallest eigenvalues and the lowermost figure is the four largest eigenvalues. Surprisingly, every eigenvalue decreases when the coupling coefficient increases, meaning that every direction gets harder to control. The trace of the Gramian with varying coupling coefficient is depicted in Figure 5.4.

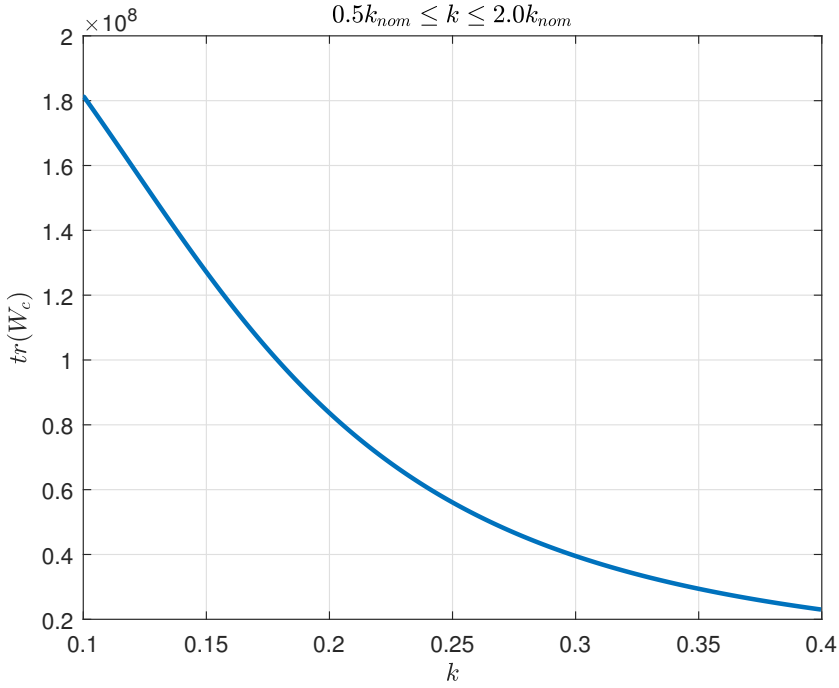

Figure 5.4: Trace of the Gramian with varying coupling coefficient.

Not surprisingly, the average controllability decreases since every eigenvalue also decreases.

All other possible eigenvalue trajectories and trace curves of the controllability Gramian with varying dynamic parameters are reported in Appendix B.

5.3 Analysis of the observability Gramian

There are several ways of measuring and to interpret the degree of observability as well, by analyzing the observability Gramian. Depending on complexity, cost, safety and so on, different output configurations are possible, i.e. which states to measure.

5.3.1 Measuring all currents

A possible output configuration is to have a measurement on the currents flowing in the system. Thus, the output matrix $\boldsymbol{C}$ is as follows:

$$\boldsymbol{C} = diag(\begin{bmatrix} 1 & 1 & 1 & 1 & 0 & 0 & 0 & 0 \end{bmatrix}) \tag{5.34}$$

The observability measures are found as:

$$\lambda_{min}(\boldsymbol{W}_o) = 3.3694 \cdot 10^{-9} \tag{5.35a}$$
$$tr(\boldsymbol{W}_o) = 2.3262 \cdot 10^{-4} \tag{5.35b}$$
$$V(\mathcal{E}_{min}) = 0.0031 \tag{5.35c}$$

5.3.2 Measuring the sending side currents

It is also interesting to evaluate the case when having measurement only on the sending side currents. In this case, the output matrix $\boldsymbol{C}$ reads:

$$\boldsymbol{C} = diag(\begin{bmatrix} 1 & 1 & 0 & 0 & 0 & 0 & 0 & 0 \end{bmatrix}) \tag{5.36}$$

The observability measures are in this case:

$$\lambda_{min}(\boldsymbol{W}_o) = 4.8756 \cdot 10^{-10} \tag{5.37a}$$
$$tr(\boldsymbol{W}_o) = 4.9114 \cdot 10^{-5} \tag{5.37b}$$
$$V(\mathcal{E}_{min}) = 0.0013 \tag{5.37c}$$

5.3.3 Measuring the receiving side currents

In this case, the output matrix $\boldsymbol{C}$ reads:

$$\boldsymbol{C} = diag(\begin{bmatrix} 0 & 0 & 1 & 1 & 0 & 0 & 0 & 0 \end{bmatrix}) \tag{5.38}$$

and the observability measures are:

$$\lambda_{min}(\boldsymbol{W}_o) = 2.3243 \cdot 10^{-9} \tag{5.39a}$$
$$tr(\boldsymbol{W}_o) = 1.8350 \cdot 10^{-4} \tag{5.39b}$$
$$V(\mathcal{E}_{min}) = 0.0027 \tag{5.39c}$$

5.3.4 Measuring the sending side states

Another possible output configuration is to have a measurement only on the sending side. Thus, the output matrix $\boldsymbol{C}$ is as follows:

$$\boldsymbol{C} = diag(\begin{bmatrix} 1 & 1 & 0 & 0 & 1 & 1 & 0 & 0 \end{bmatrix}) \tag{5.40}$$

Now, the observability measures are calculated as:

$$\lambda_{min}(\boldsymbol{W}_o) = 4.0861 \cdot 10^{-6} \tag{5.41a}$$
$$tr(\boldsymbol{W}_o) = 0.4332 \tag{5.41b}$$
$$V(\mathcal{E}_{min}) = 0.1209 \tag{5.41c}$$

5.3.5 Measuring the receiving side states

It is interesting to evaluate the case when having a measurement only on the receiving side as well. In this case, the output matrix $\boldsymbol{C}$ reads:

$$\boldsymbol{C} = diag(\begin{bmatrix} 0 & 0 & 1 & 1 & 0 & 0 & 1 & 1 \end{bmatrix}) \tag{5.42}$$

The observability measures are in this case:

$$\lambda_{min}(\boldsymbol{W}_o) = 1.0995 \cdot 10^{-6} \tag{5.43a}$$
$$tr(\boldsymbol{W}_o) = 0.0913 \tag{5.43b}$$
$$V(\mathcal{E}_{min}) = 0.0589 \tag{5.43c}$$

5.3.6 Measuring all states

When measuring every state, the output matrix $\boldsymbol{C}$ reads:

$$\boldsymbol{C} = diag(\begin{bmatrix}1 & 1 & 1 & 1 & 1 & 1 & 1 & 1\end{bmatrix}) \tag{5.44}$$

The observability measures are in this case as follows:

$$\lambda_{min}(\boldsymbol{W}_o) = 6.3140 \cdot 10^{-6} \tag{5.45a}$$
$$tr(\boldsymbol{W}_o) = 0.5245 \tag{5.45b}$$
$$V(\mathcal{E}_{min}) = 0.1376 \tag{5.45c}$$

5.3.7 Summary of observability Gramian measures

Table 5.2: SUMMARY OF OBSERVABILITY GRAMIAN MEASURES

Measurement	$\lambda_{min}(\boldsymbol{W}_o)$	$tr(\boldsymbol{W}_o)$	$V(\mathcal{E}_{min})$
Currents	$3.3694 \cdot 10^{-9}$	$2.3262 \cdot 10^{-4}$	0.0031
Sen. currents	$4.8756 \cdot 10^{-10}$	$4.9114 \cdot 10^{-5}$	0.0013
Rec. currents	$2.3243 \cdot 10^{-9}$	$1.8350 \cdot 10^{-4}$	0.0027
Sending side	$4.0861 \cdot 10^{-6}$	0.4332	0.1209
Receiving side	$1.0995 \cdot 10^{-6}$	0.0913	0.0589
Every state	$6.3140 \cdot 10^{-6}$	0.5245	0.1376

Not surprisingly, measuring all state variable yields the best observability, whereas having measurements only on the sending currents results in the worst observability metrics. It can also be noted that observing all sending side states results in better overall observability than observing the receiving side states, whereas measuring the receiving side currents gives better observability than measuring the sending side currents.

All eigenvalue trajectories and trace curves of the observability Gramian with varying dynamic parameters are reported in Appendix C.

5.4 Transfer functions and potential of model order reduction

Lower-order systems are well recognized and easy to understand in terms of characteristics such as settling time, damping, time constants, oscillations and so on. High-order systems are more complex and harder to manipulate and work with relative to lower-order models when e.g. conducting analysis and design of controllers. Therefore, model order reduction could prove very useful when dealing with high-order systems. Techniques such as dominant pole approximation and discarding states that do not influence the dynamic behavior of the system could be applied in order to obtain such a reduction. It is, however, important that the reduced-order model conserves the dynamic properties and characteristics of the full-order model that is important for the application of the system in question. Thus, verification of the behavior of the reduced-order model in e.g. frequency- and time-domain is crucial.

5.4.1 Second-order approximation

Since the linearized model consists of four input signals and potential eight output signals, there exists up to thirty-two input-output transfer functions. Only one of them is focused on in the following.

The eight-order transfer function from $v_{1,d}$ to $i_{2,q}$ reads:

$$\left[\frac{1.31\cdot10^{9}s^{6}-0.99s^{5}+3.42\cdot10^{20}s^{4}-1.39\cdot10^{26}s^{3}-4.48\cdot10^{32}s^{2}-3.95\cdot10^{37}s-1.30\cdot10^{42}}{s^{8}+1.89\cdot10^{5}s^{7}+2.33\cdot10^{12}s^{6}+3.28\cdot10^{17}s^{5}+1.35\cdot10^{24}s^{4}+1.28\cdot10^{29}s^{3}+8.56\cdot10^{33}s+3.66\cdot10^{38}s}\right] \tag{5.46}$$

The frequency and step response for this transfer function is displayed in Figure 5.5.

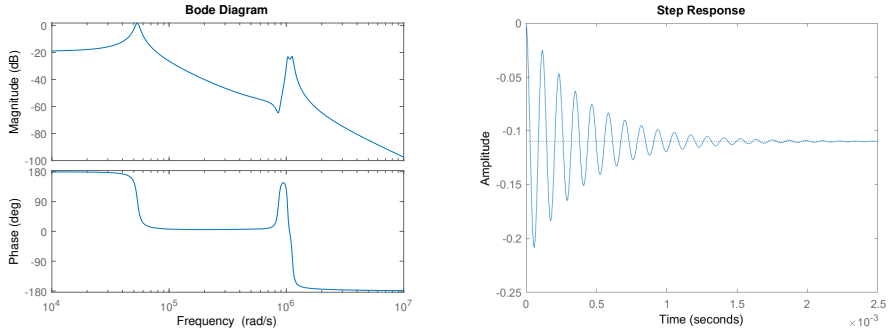

Figure 5.5: Frequency and step response for transfer function from $v_{1.d}$ to $i_{2,q}$.

Since the system is oscillating due to complex poles, a first-order approximation using e.g. Skogestad's method is impossible. However, by looking at the bode plot and the step response, a second-order transfer function of the form:

$$H_{app}(s) = k\frac{\omega_n^2}{s^2 + 2\zeta\omega_n s + \omega_n^2} \tag{5.47}$$

where k is the dc-gain gain, ζ is the damping ratio and ω_n is the natural frequency, could potentially give a reasonable approximation in a certain frequency interval.

The second-order transfer function with $k = -0.11$, $\omega_n = 5.39\cdot10^4$ and $\zeta = 0.047$ is depicted in the same bode diagram as the original eight-order transfer function, in Figure 5.6. In addition, the response to a step input signal for both transfer functions are displayed in Figure 5.7

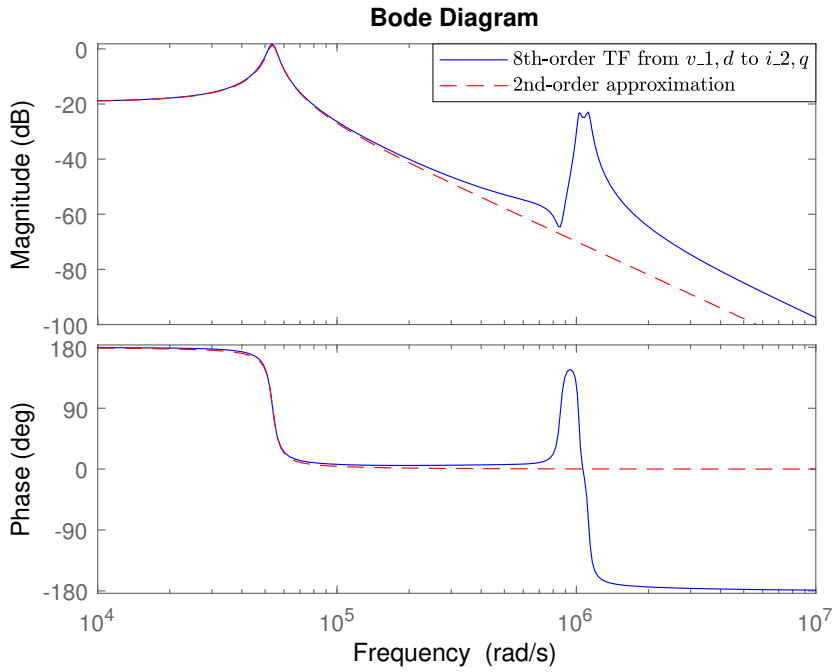

Figure 5.6: Frequency response of original and second-order approximate transfer function.

It is clear that the second-order approximation $H_{app}(s)$ could quite accurately capture the dynamics of the eight-order transfer function up until a frequency of $\approx 400\ 000$ rad/s.

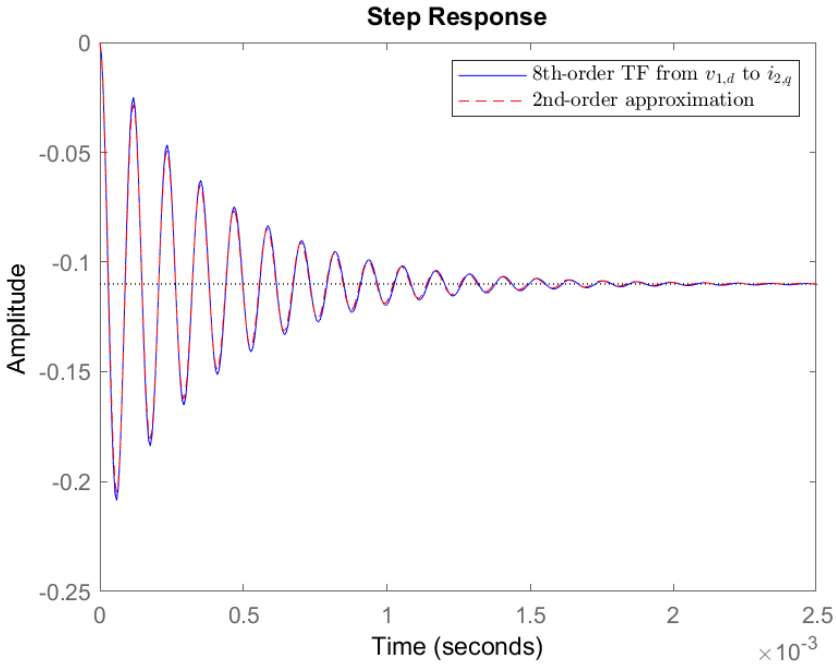

Figure 5.7: Step response of original and second-order approximate transfer function.

It is obvious that the second-order approximation captures the behavior of the eight-order system's response to a step input signal.

The poles of the second-order is found to be:

$$eig(H_{app}(s)) = -2728 \pm i53840 \tag{5.48}$$

The most dominant pole pair, i.e. the poles with the lowest real part in terms of absolute value, of the eight-order system is found in equation 4.8 as $-2949 \pm i53551$. Comparing the poles of the second-order system to the original eight-order system reveals that they are almost the same, meaning that this pole pair significantly dominates the response of the original system and that it does not exist any zeros in close proximity that reduces the influence of the poles.

5.4.2 Fourth-order approximation

A fourth-order approximation could in addition capture the second resonance peak observed in the bode diagram in Figure 5.5. The bode diagram and step response of the fourth-order transfer function:

$$H_{app2}(s) = \frac{2476s^3 + 3.26 \cdot 10^8 s^2 - 3.56 \cdot 10^{14} s - 3.66 \cdot 10^{20}}{s^4 + 32010s^3 + 1.16 \cdot 10^{12} s^2 + 6.80 \cdot 10^{15} s + 3.33 \cdot 10^{21}} \quad (5.49)$$

is depicted together with the original eight-order transfer function in Figure 5.8 and 5.9, respectively.

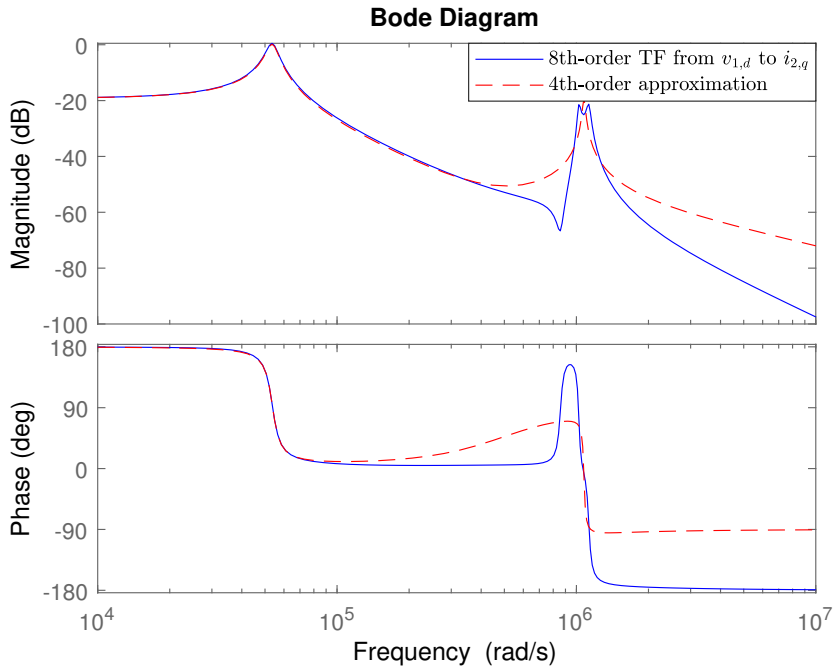

Figure 5.8: Frequency response of original and fourth-order approximate transfer function.

As expected, the fourth-order transfer function gives a reasonable approximation around the second resonance peak in addition to an accurate approximation for

lower frequencies.

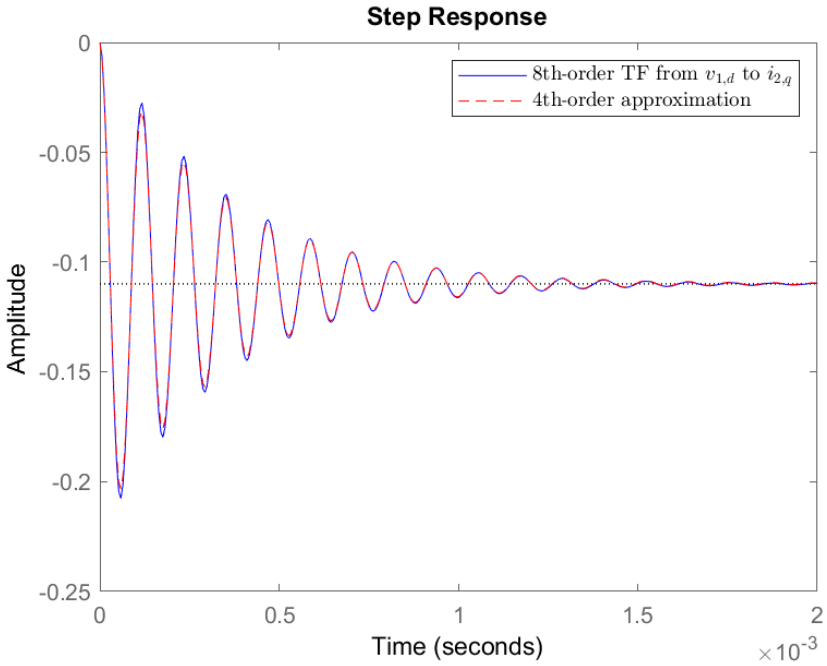

Figure 5.9: Step response of original and fourth-order approximate transfer function.

As for the second-order approximation, the fourth-order also captures the behavior of the eight-order system's response to a step input signal.

The goes to show that there exist possibilities of model order reduction of this system. One technique for obtaining a lower-order model that preserves the dynamics of interest is the balanced truncation model reduction strategy. The main idea with this technique is to calculate a balanced realization of the system, using both observability and controllability Gramian, and thereby address and eliminate the states x that are difficult to control and observe at the same time.

Every transfer function of the model is reported in Appendix D.

Chapter 6

Conclusion and Future Work

6.1 Conclusion

A linearizable nonlinear state-space model of an inductive power transfer system has been analyzed. In order for the model to arrive at a constant equilibrium point in steady-state, the model is represented in a synchronous reference frame by utilization of the Park transform. Linearization of the model is performed in an operating point corresponding to the steady-state equilibrium, allowing for various stability analysis methods to be utilized.

Several configurations regarding the input variables in the model have been investigated in order to provide an understanding of how the controllability depends upon the inputs. This investigation has revealed the differences in controllability when the system's input configuration is modified. Best overall controllability is achieved when having control on both sides, whereas controlling only the sending side d-axis voltage results in the worst controllability metrics. It has also revealed that some input variables only gives a minor contribution to overall controllability. Analysis of the observability Gramian has demonstrated the variation in observability with different output configurations. Furthermore, eigenvalue analysis has been conducted, and it has been established that there exists a pole pair, a critical mode, with noteworthy lower damping and higher settling time than the rest. Calculation of participation factors has illustrated which states that have the highest impact on this critical mode, which implies the importance of considering these

states when potential design and analysis of control strategies is to be made. Furthermore, investigation of transfer functions has revealed that there exist possibilities of model order reduction, which could greatly simplify the model and prove very useful in further analysis and control design.

6.2 Future work

This report should be reviewed as a preparation study that can form a basis for new developments in the research field of inductive power transfer. Several different tests and experiments have been left out due to lack of time. Thus, additional analysis of small-signal characteristics with various system conditions could be done, in order to assess their importance and applicability in e.g. new developments and expansion of the model. As an example, parameter sensitivities could be explored, i.e. matrices that describes how sensitive the eigenvalues are to changes in the parameters of the system. In addition, in-depth study of the different transfer functions describing the system dynamics could be made, in order to find potential lower order approximations with similar dynamics and steady-state characteristics. Furthermore, developing a model in MATLAB/Simscape/Simulink and perform simulations and tests could provide important information regarding the dynamics of the model and could help in the future potential design of control systems. Analysis of the system in off-resonant operation could in addition provide further understanding regarding possible control design and system dynamics.

Bibliography

[1] Giuseppe Guidi and Jon Are. ”Modelling techniques for designing high-performance on-road dynamic charging systems for electric vehicles”. 2018.

[2] Grant A. Covic and John T. Boys. ”Inductive power transfer”. *Proceedings of the IEEE*, 101(6):1276–1289, 2013.

[3] Grant Anthony Covic and John T. Boys. ”Modern trends in inductive power transfer for transportation applications”. *IEEE Journal of Emerging and Selected Topics in Power Electronics*, 1:28–41, 2013.

[4] Y. Hori K. Hata, T. Imura. ”Dynamic wireless power transfer system for electric vehicle to simplify ground facilities”. *EVS28 International Electric Vehicle Symposium and Exhibition*, 7:1–12, 2015.

[5] F. Viola P. Romano R. Miceli M. Longo, D. Zaninelli. ”How is the spread of the electric vehicles?”. (4), 2015.

[6] By Giuseppe Guidi, Jon Are Suul, and Frode Jenset. Wireless Charging for Ships. *IEEE Electrification Magazine*, (september):22–32, 2017.

[7] A.W. Green. ”10 kHz inductively coupled power transfer - concept and control”. *Proceedings of 5th International Conference on Power Electronics and Variable-Speed Drives*, 1994(399):694–699, 1994.

[8] Wei Zhang and Chunting Chris Mi. ”Compensation topologies of high-power wireless power transfer systems”. *IEEE Transactions on Vehicular Technology*, 65(6):4768–4778, 2016.

[9] Chunting Chris Mi, Giuseppe Buja, Su Y. Choi, and Chun T. Rim. "Modern advances in wireless power transfer systems for roadway powered electric vehicles". *IEEE Transactions on Industrial Electronics*, 63(10):6533–6545, 2016.

[10] Kunwar Aditya and Sheldon S. Williamson. "Comparative study of Series-Series and series-parallel compensation topologies for electric vehicle charging". *IEEE International Symposium on Industrial Electronics*, pages 426–430, 2014.

[11] Giuseppe Guidi and Jon Are Suul. "Minimizing converter requirements of inductive power transfer systems with constant voltage load and variable coupling conditions". *IEEE Transactions on Industrial Electronics*, 63(11):6835–6844, 2016.

[12] Roman Bosshard, Johann Walter Kolar, Jonas Mühlethaler, Ivica Stevanović, Bernhard Wunsch, and Francisco Canales. "Modeling and η - α-pareto optimization of inductive power transfer coils for electric vehicles". *IEEE Journal of Emerging and Selected Topics in Power Electronics*, 3(1):50–64, 2015.

[13] Andrew Foote and Omer C. Onar. "A review of high-power wireless power transfer". *2017 IEEE Transportation and Electrification Conference and Expo, ITEC 2017*, pages 234–240, 2017.

[14] Chi-Tsong Chen. *"Linear system theory and design, 3th edition"*. Oxford University Press, Inc, 1999.

[15] John Lygeros Tyler H. Summers, Fabrizio L. Cortesi. "On submodularity and controllability in complex dynamical networks". *IEEE transactions on control of network systems*, Vol. 3(1):pp. 91–101, March 2016.

[16] Fabrizio L. Cortesi, Tyler H. Summers, and John Lygeros. "Submodularity of energy related controllability metrics". *Proceedings of the IEEE Conference on Decision and Control*, 2015(February):2883–2888, 2014.

[17] Franco Garofalo, Luigi Iannelli, and Francesco Vasca. "Participation factors and their connections to residues and relative gain array". *IFAC Proceedings Volumes (IFAC-PapersOnline)*, 15(1):125–130, 2002.

[18] Wael A. Hashlamoun, Munther A. Hassouneh, and Eyad H. Abed. "New results on modal participation factors: Revealing a previously unknown

dichotomy". *IEEE Transactions on Automatic Control*, 54(7):1439–1449, 2009.

Appendix A

Matlab Code

Overview of the main MATLAB files used in this report is presented in Table A.1. The table includes a short description of the scripts, and the dependencies-column state which scripts the particular MATLAB file uses.

Table A.1: OVERVIEW OF MATLAB-FILES

Filename	Description	Dependencies
parameters.m	Assign values to parameters	None
getSteadyStateSol.m	Returns symbolic steady-state	None
getSymStateSpace.m	Returns symbolic state-space	getSteadyStateSol.m
getNumStateSpace.m	Returns numerical state-space	parameters.m getSymStateSpace.m
eigTrajectory_Vdc.m	Plots eigenvalue trajectories of A matrix	parameters.m getSymStateSpace.m
eigTrajectory_k.m	Plots eigenvalue trajectories of A matrix	parameters.m getSymStateSpace.m
eigTrajectoryGr_Vdc.m	Plots eigenvalue trajectories of Gramian	parameters.m getSymStateSpace.m getNumStateSpace.m
eigTrajectoryGr_k.m	Plots eigenvalue trajectories of Gramian	parameters.m getSymStateSpace.m getNumStateSpace.m
participationFactor.m	Finds participation factors	getNumStateSpace.m

```
%% Parameters

P_0 = 10*10^(3);
f_0 = 85*10^(3);
k_nom = 0.2;
omega_0 = 2*pi*f_0;

% Primary coil
V_1nom = 380;
L_1 = 176*10^(-6);
Q_1 = 310;
R_1 = omega_0*L_1/Q_1;
C_1 = 1/(L_1*omega_0^(2));

% Secondary coil
V_2nom = 235;
L_2 = 41*10^(-6);
Q_2 = 270;
R_2 = omega_0*L_2/Q_2;
C_2 = 1/(L_2*omega_0^(2));

% Mutual
M = k_nom*sqrt(L_1*L_2);
L_alpha1 = L_1 - M^(2)/L_2;
L_alpha2 = L_2 - M^(2)/L_1;

% Input variables
V_10 = V_1nom;
V_dcout = pi/4*V_2nom;

filename = 'parameters';
save(filename);
```

Listing A.1: Assign values to parameters

```
function [i_1d0, i_1q0, i_2d0, i_2q0, v_c1d0, v_c1q0, v_c2d0,
    v_c2q0] = getSteadyStateSol()
    pi =sym('pi');
    M = sym('M','positive');
    R_1 = sym('R_1','positive');
    R_2 = sym('R_1','positive');
    L_1 = sym('L_1','positive');
    L_2 = sym('L_2','positive');
    C_1 = sym('C_1','positive');
    C_2 = sym('C_2','positive');
    L_alpha1 = sym('L_alpha1','positive');
    L_alpha2 = sym('L_alpha2','positive');
    omega = sym('omega','positive');
    omega_0 = sym('omega_0','positive');
    syms i_1d i_1q i_2d i_2q v_c1d v_c1q v_c2d v_c2q v_1d v_1q
    V_dcout

    %% Main model

    f1 = omega*i_1q + (-R_1*i_1d + M*R_2/L_2*i_2d - v_c1d + M/L_2*
    v_c2d + ...
    v_1d + M/L_2*i_2d*4/pi*V_dcout/sqrt(i_2d^(2) + i_2q^(2)))/
    L_alpha1 == 0;

    f2 = -omega*i_1d + (-R_1*i_1q + M*R_2/L_2*i_2q - v_c1q + M/L_2
    *v_c2q + ...
    v_1q + M/L_2*i_2q*4/pi*V_dcout/sqrt(i_2d^(2) + i_2q^(2)))/
    L_alpha1 == 0;

    f3 = omega*i_2q + (M*R_1/L_1*i_1d - R_2*i_2d + M/L_1*v_c1d -
    v_c2d - ...
    M/L_1*v_1d - i_2d*4/pi*V_dcout/sqrt(i_2d^(2) + i_2q^(2)))/
    L_alpha2 == 0;

    f4 = -omega*i_2d + (M*R_1/L_1*i_1q - R_2*i_2q + M/L_1*v_c1q -
    v_c2q - ...
    M/L_1*v_1q - i_2q*4/pi*V_dcout/sqrt(i_2d^(2) + i_2q^(2)))/
    L_alpha2 == 0;

    f5 = omega*v_c1q + 1/C_1*i_1d == 0;

    f6 = -omega*v_c1d + 1/C_1*i_1q == 0;

    f7 = omega*v_c2q + 1/C_2*i_2d == 0;
```

```
35
36      f8 = -omega*v_c2d + 1/C_2*i_2q == 0;
37
38      % Solve voltages in terms of currents
39      eqns = [f5, f6, f7, f8];
40      vars = [v_c1d, v_c1q, v_c2d, v_c2q];
41      solVoltage = solve(eqns, vars);
42
43      v_c1d0 = solVoltage.v_c1d;
44      v_c1q0 = solVoltage.v_c1q;
45      v_c2d0 = solVoltage.v_c2d;
46      v_c2q0 = solVoltage.v_c2q;
47
48      % Substitution of steady-state voltages
49      f1 = subs(f1, v_c1d, v_c1d0);
50      f1 = subs(f1, v_c2d, v_c2d0);
51
52      f2 = subs(f2, v_c1q, v_c1q0);
53      f2 = subs(f2, v_c2q, v_c2q0);
54
55      f3 = subs(f3, v_c1d, v_c1d0);
56      f3 = subs(f3, v_c2d, v_c2d0);
57
58      f4 = subs(f4, v_c1q, v_c1q0);
59      f4 = subs(f4, v_c2q, v_c2q0);
60
61      % Substitution of R_eq
62      syms R_eq
63      f1 = subs(f1, 4/pi*V_dcout/sqrt(i_2d^(2) + i_2q^(2)), R_eq);
64      f2 = subs(f2, 4/pi*V_dcout/sqrt(i_2d^(2) + i_2q^(2)), R_eq);
65      f3 = subs(f3, 4/pi*V_dcout/sqrt(i_2d^(2) + i_2q^(2)), R_eq);
66      f4 = subs(f4, 4/pi*V_dcout/sqrt(i_2d^(2) + i_2q^(2)), R_eq);
67
68      % Assumptions
69      V_10 = sym('V_10','positive');
70      v_1d = V_10;
71      v_1q = 0;
72
73      % Single resonant frequency
74      omega = 1/sqrt(L_1*C_1);
75      C_1 = C_2*L_2/L_1;
76
77      % Leakage factors
78      L_alpha1 = L_1 - M^2/L_2;
79      L_alpha2 = L_2 - M^2/L_1;
```

```
80
81      % Solution of steady-state currents
82      eqns2 = [f1, f2, f3, f4];
83      vars2 = [i_1d, i_1q, i_2d, i_2q];
84      solCurrent = solve(eqns2, vars2);
85
86      i_1d0 = solCurrent.i_1d;
87      i_1q0 = solCurrent.i_2d;
88      i_2d0 = solCurrent.i_1q;
89      i_2q0 = solCurrent.i_2q;
90
91      % Simplify
92      i_1d0 = eval(simplify(i_1d0));
93      i_1q0 = eval(simplify(i_1q0));
94      i_2d0 = eval(simplify(i_2d0));
95      i_2q0 = eval(simplify(i_2q0));
96
97      % Assume negligible losses
98      R_1 = 0;
99      R_2 = 0;
100
101     % Simplify further
102     i_1d0 = eval(simplify(i_1d0));
103     i_1q0 = eval(simplify(i_1q0));
104     i_2d0 = eval(simplify(i_2d0));
105     i_2q0 = eval(simplify(i_2q0));
106
107     % i_1q0 and i_2d0 is zero and not treated further
108
109     % Substitution of resonant frequency
110     i_1d0 = subs(i_1d0, C_2*L_2, 1/omega_0^2);
111     i_2q0 = subs(i_2q0, C_2*L_2, 1/omega_0^2);
112
113     % Substitution of R_eq
114     syms I_2
115     R_eq = 4/pi*V_dcout/I_2;
116
117     % Simplify
118     i_1d0 = eval(simplify(i_1d0));
119
120     % Substitution of I_2
121     I_2 = V_10/(omega_0*M);
122
123     % Final simplification;
124     i_1d0 = eval(simplify(i_1d0));
```

```
125     i_2q0 = eval(simplify(i_2q0));
126
127     % Substitute steady-state resonant frequency
128     syms omega % Force omega to be variable
129     v_c1d0 = subs(v_c1d0, omega, omega_0);
130     v_c1q0 = subs(v_c1q0, omega, omega_0);
131     v_c2d0 = subs(v_c2d0, omega, omega_0);
132     v_c2q0 = subs(v_c2q0, omega, omega_0);
133
134     % Substitution of steady-state currents
135     v_c1d0 = subs(v_c1d0, i_1q, i_1q0);
136     v_c1q0 = subs(v_c1q0, i_1d, i_1d0);
137     v_c2d0 = subs(v_c2d0, i_2q, i_2q0);
138     v_c2q0 = subs(v_c2q0, i_2d, i_2d0);
139
140 end
```

Listing A.2: Returns steady-state solutions

```
function [A, B] = getSymStateSpace()
    %% Symbolic variables and constants

    M = sym('M','positive');
    R_1 = sym('R_1','positive');
    R_2 = sym('R_2','positive');
    L_1 = sym('L_1','positive');
    L_2 = sym('L_2','positive');
    C_1 = sym('C_1','positive');
    C_2 = sym('C_2','positive');
    L_alpha1 = sym('L_alpha1','positive');
    L_alpha2 = sym('L_alpha2','positive');
    omega = sym('omega','positive');
    omega_0 = sym('omega_0','positive');

    syms i_1d i_1q i_2d i_2q v_c1d v_c1q v_c2d v_c2q v_1d v_1q
    V_dcout

    %% Nonlinear model

    f1 = omega*i_1q + (-R_1*i_1d + M*R_2/L_2*i_2d - v_c1d + M/L_2*
    v_c2d + ...
    v_1d + M/L_2*i_2d/sqrt(i_2d^(2) + i_2q^(2))*4/pi*V_dcout)/
    L_alpha1;

    f2 = -omega*i_1d + (-R_1*i_1q + M*R_2/L_2*i_2q - v_c1q + M/L_2
    *v_c2q + ...
    v_1q + M/L_2*i_2q/sqrt(i_2d^(2) + i_2q^(2))*4/pi*V_dcout)/
    L_alpha1;

    f3 = omega*i_2q + (M*R_1/L_1*i_1d - R_2*i_2d + M/L_1*v_c1d -
    v_c2d  - ...
    M/L_1*v_1d - i_2d/sqrt(i_2d^(2) + i_2q^(2))*4/pi*V_dcout)/
    L_alpha2;

    f4 = -omega*i_2d + (M*R_1/L_1*i_1q - R_2*i_2q + M/L_1*v_c1q -
    v_c2q - ...
    M/L_1*v_1q - i_2q/sqrt(i_2d^(2) + i_2q^(2))*4/pi*V_dcout)/
    L_alpha2;

    f5 = omega*v_c1q + 1/C_1*i_1d;

    f6 = -omega*v_c1d + 1/C_1*i_1q;

```

```
36      f7 = omega*v_c2q + 1/C_2*i_2d;
37
38      f8 = -omega*v_c2d + 1/C_2*i_2q;
39
40      %% Linearization
41
42      A = jacobian([f1;f2;f3;f4;f5;f6;f7;f8], [i_1d i_1q i_2d i_2q
        v_c1d v_c1q v_c2d v_c2q]);
43      B = jacobian([f1;f2;f3;f4;f5;f6;f7;f8], [v_1d v_1q omega
        V_dcout]);
44
45      % Get steady-state solutions
46      [i_1d0, i_1q0, i_2d0, i_2q0, v_c1d0, v_c1q0, v_c2d0, v_c2q0] =
         getSteadyStateSol();
47
48      % Steady-state assignment
49      i_1d = i_1d0;
50      i_1q = i_1q0;
51      i_2d = i_2d0;
52      i_2q = i_2q0;
53      v_c1d = v_c1d0;
54      v_c1q = v_c1q0;
55      v_c2d = v_c2d0;
56      v_c2q = v_c2q0;
57      omega = omega_0;
58
59      % Evaluate and simplify
60      A = eval(simplify(A));
61      A = simplify(A);
62      B = eval(simplify(B));
63      B = simplify(B);
64
65  end
```

Listing A.3: Returns Symbolic state-space

```
function [Ad, Bd, Cd, Dd] = getNumStateSpace()
    % Get parameters
    load('parameters.mat');

    % Get symbolic state-space
    [A, B] = getSymStateSpace();

    %% State space matrices
    Ad = eval(A);
    Bd = eval(B);
    Cd = eye(length(A));
    Dd = 0;
end
```

Listing A.4: Returns numerical state-space

```
% Get parameters
load('parameters.mat')

% Get symbolic state-space
[A, B] = getSymStateSpace();

% Assumptions
v_1d = V_10;
v_1q = 0;

%% Eigenvalues with varying load conditions

N = 1000;
eigTable = zeros(8, N);
inc = 1.5*V_dcout/ N;
V_2min = 0.5*V_2nom;
V_dcoutmin = pi/4*V_2min;
V_dcout = V_dcoutmin;
for i = 1:N
    Aeval = eval(A);
    Eigenvalues = eig(Aeval);
    eigTable(:, i) = Eigenvalues;
    V_dcout = V_dcout + inc;
end
V_dcoutmax = V_dcout;
V_2max = 4/pi*V_dcoutmax;
trans = eigTable';
realEig = real(trans);
imagEig = imag(trans);

%% Plotting of eigenvalue trajectories

figure()
hold on
grid on
for i = 1:8
    scatter(realEig(:,i), imagEig(:,i), 1, 'b');
end
xlabel('Real part')
ylabel('Imaginary part')
scatter(realEig(1,:), imagEig(1,:), 'o', 'b');
scatter(realEig(N,:), imagEig(N,:), 'v', 'r');
title('$0.5V_{2,nom} \leq V_2 \leq 2V_{2,nom}$', 'interpreter', '
    latex');
```

Listing A.5: Plots eigenvalue trajectories of A-matrix with varying load

```
% Get parameters
load('parameters.mat')

% Get symbolic state-space
[A, B] = getSymStateSpace();

% Assumptions
v_1d = V_10;
v_1q = 0;

%% Eigenvalues with varying coupling conditions

N = 1000;
eigTable = zeros(8, N);
inc = 1.5*k_nom/N;
kmin = 0.5*k_nom;
Mmin = kmin*sqrt(L_1*L_2);
k_nom = kmin;
for i = 1:N
    M = k_nom*sqrt(L_1*L_2);
    L_alpha1 = L_1 - M^(2)/L_2;
    L_alpha2 = L_2 - M^(2)/L_1;
    Aeval = eval(A);
    Eigenvalues = eig(Aeval);
    eigTable(:, i) = Eigenvalues;
    k_nom = k_nom + inc;
end
kmax = k_nom;
Mmax = kmax*sqrt(L_1*L_2);
trans = eigTable';
realEig = real(trans);
imagEig = imag(trans);

%% Plotting of eigenvalue trajectories

figure()
hold on
grid on
for i = 1:8
    scatter(realEig(:,i), imagEig(:,i), 1, 'b');
end
xlabel('Real part')
ylabel('Imaginary part')
scatter(realEig(1,:), imagEig(1,:), 'o', 'b');
```

```
45 scatter(realEig(N,:), imagEig(N,:), 'v', 'r');
46 title('$0.5k_{nom} \leq k \leq 2.0k_{nom}$','Interpreter','latex')
       ;
```

Listing A.6: Plots eigenvalue trajectories of A-matrix with varying coupling coefficient

```
% Get parameters
load('parameters.mat')

% Get symbolic state-space
[A, B] = getSymStateSpace();

% Get C and D matrices
[~, ~, C, D] = getNumStateSpace();

% Assumptions
v_1d = V_10;
v_1q = 0;

%% Eigenvalues with varying load conditions

N = 1000;
traceVec = zeros(1,N);
V_dcoutvec = zeros(1,N);
eigTable = zeros(8, N);
inc = 1.5*V_dcout/ N;
V_2min = 0.5*V_2nom;
V_dcoutmin = pi/4*V_2min;
V_dcout = V_dcoutmin;
for i = 1:N
    Aeval = eval(A);
    Beval = eval(B);
    sys = ss(Aeval, Beval, C, D);
    Wc = gram(sys,'c');
    Eigenvalues = eig(Wc);
    eigTable(:, i) = Eigenvalues;
    V_dcoutvec(i) = V_dcout;
    traceVec(i) = trace(Wc);
    V_dcout = V_dcout + inc;

end
V_2max = 4/pi*V_dcout;
trans = eigTable';
realEig = real(trans);
imagEig = imag(trans);

%% Plotting of eigenvalue trajectories
subplot(2,1,1)
hold on
grid on
```

```
45 for i = 1:4
46     scatter(realEig(:,i), imagEig(:,i), 1, 'b');
47 end
48 xlabel('Real part')
49 ylabel('Imaginary part')
50 scatter(realEig(1,1:4), imagEig(1,1:4), 'o', 'b');
51 scatter(realEig(N,1:4), imagEig(N,1:4), 'v', 'r');
52 title('$0.5V_{2,nom} \leq V_2 \leq 2V_{2,nom}$', 'interpreter', '
       latex');
53
54 subplot(2,1,2)
55 hold on
56 grid on
57 for i = 5:8
58     scatter(realEig(:,i), imagEig(:,i), 1, 'b');
59 end
60 xlabel('Real part')
61 ylabel('Imaginary part')
62 scatter(realEig(1,5:8), imagEig(1,5:8), 'o', 'b');
63 scatter(realEig(N,5:8), imagEig(N,5:8), 'v', 'r');
64
65 figure()
66 plot(V_dcoutvec, traceVec, 'LineWidth', 2);
67 xlabel('$V_{dc,out}$', 'interpreter', 'latex')
68 ylabel('$tr(W_c)$', 'interpreter', 'latex')
69 title('$0.5V_{2,nom} \leq V_2 \leq 2V_{2,nom}$', 'interpreter', '
       latex');
70 grid on
```

Listing A.7: Plots eigenvalue trajectories and trace of Gramian with varying load

```
% Get parameters
load('parameters');

% Get symbolic state-space
[A, B] = getSymStateSpace();

% Get C and D matrices
[~, ~, C, D] = getNumStateSpace();

% Assumptions
v_1d = V_10;
v_1q = 0;

%% Eigenvalues with varying coupling conditions

N = 1000;
traceVec = zeros(1,N);
k_vec = zeros(1,N);
eigTable = zeros(8, N);
inc = 1.5*k_nom/N;
kmin = 0.5*k_nom;
Mmin = kmin*sqrt(L_1*L_2);
k_nom = kmin;
for i = 1:N
    M = k_nom*sqrt(L_1*L_2);
    L_alpha1 = L_1 - M^(2)/L_2;
    L_alpha2 = L_2 - M^(2)/L_1;
    Aeval = eval(A);
    Beval = eval(B);
    sys = ss(Aeval, Beval, C, D);
    Wc = gram(sys,'c');
    Eigenvalues = eig(Wc);
    eigTable(:, i) = Eigenvalues;
    k_vec(i) = k_nom;
    traceVec(i) = trace(Wc);
    k_nom = k_nom + inc;
end
kmax = k_nom;
Mmax = kmax*sqrt(L_1*L_2);
trans = eigTable';
realEig = real(trans);
imagEig = imag(trans);

%% Plotting of eigenvalue trajectories
```

```
45
46 subplot(2,1,1)
47 hold on
48 grid on
49 for i = 1:4
50     scatter(realEig(:,i), imagEig(:,i), 1, 'b');
51 end
52 xlabel('Real part')
53 ylabel('Imaginary part')
54 scatter(realEig(1,1:4), imagEig(1,1:4), 'o', 'b');
55 scatter(realEig(N,1:4), imagEig(N,1:4), 'v', 'r');
56 title('$0.5k_{nom} \leq k \leq 2.0k_{nom}$','Interpreter','latex')
       ;
57
58 subplot(2,1,2)
59 hold on
60 grid on
61 for i = 5:8
62     scatter(realEig(:,i), imagEig(:,i), 1, 'b');
63 end
64 xlabel('Real part')
65 ylabel('Imaginary part')
66 scatter(realEig(1,5:8), imagEig(1,5:8), 'o', 'b');
67 scatter(realEig(N,5:8), imagEig(N,5:8), 'v', 'r');
68
69 figure()
70 plot(k_vec, traceVec, 'LineWidth', 2);
71 xlabel('$k$', 'interpreter', 'latex')
72 ylabel('$tr(W_c)$', 'interpreter', 'latex')
73 title('$0.5k_{nom} \leq k \leq 2.0k_{nom}$','Interpreter','latex')
       ;
74 grid on
```

Listing A.8: Plots eigenvalue trajectories and trace of Gramian with varying coupling coefficient

```
[Ad, ~, ~, ~] = getNumStateSpace();

%% Modal decomposition

n = length(Ad);
[V, ~] = eig(Ad);
WT = inv(V);
W = WT';

%% Participation factor method 1

PF1 = zeros(n);
for i=1:n
    for j=1:n
        PF1(i,j) = abs(W(i,j)*V(i,j));
    end
end

%% Participation factor method 2

PF2 = zeros(n);
for i=1:n
    for j=1:n
        div = real(W(:,i))'*real(W(:,i));
        PF2(j,i) = real(W(j,i))^2/div;
    end
end


%% Participation factor method 3
% Modal decomposition, to obtain normalized left eigenvector
[~, ~, Q] = eig(Ad);

PF3 = zeros(n);
for i=1:n
    for j=1:n
        PF3(i,j) = abs(Q(i,j))^2;
    end
end

%% Participation factor method 4

PF4 = zeros(n);
for i=1:n
```

```
45      for j=1:n
46          PF4(i,j) = abs(2*real(W(i,j)*V(i,j)));
47      end
48  end
49
50  %% Parameter sensitivity to matrix entries
51
52  for i = 1:n/2
53      sens{i} = abs(W(:,2*i)*V(:,2*i)');
54  end
55
56  sens1 = cell2mat(sens(1));
57  sens2 = cell2mat(sens(2));
58  sens3 = cell2mat(sens(3));
59  sens4 = cell2mat(sens(4));
```

Listing A.9: Calculates participation factors

Appendix B

Controllability Gramian Plots

B.1 Varying load voltage

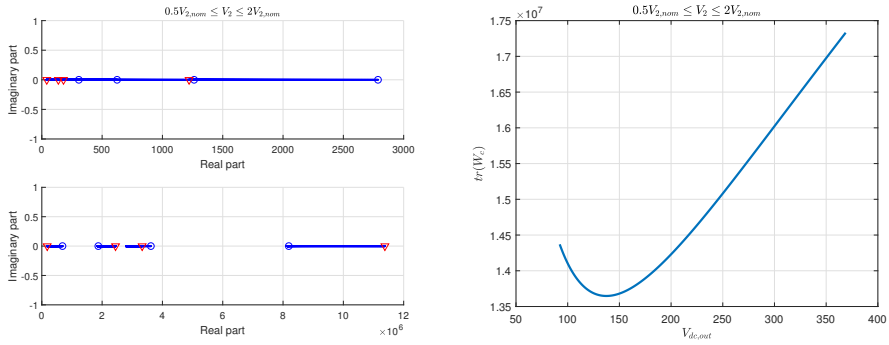

Figure B.1: Eigenvalue trajectories and trace of controllability Gramian with input only on the sending side, $v_{1,q}$ and ω considered.

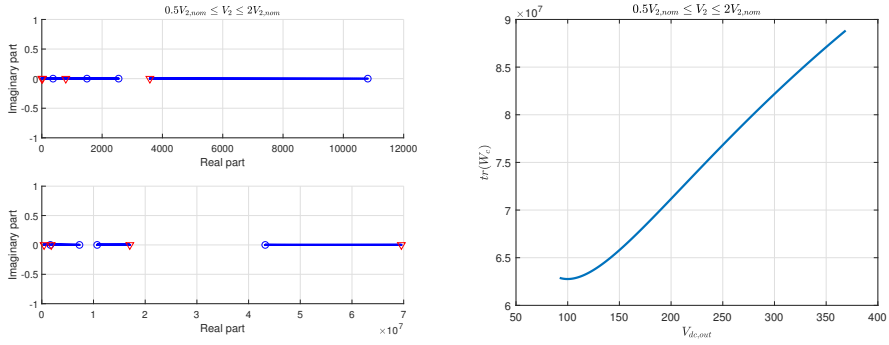

Figure B.2: Eigenvalue trajectories and trace of controllability Gramian with input only on the receiving side, $v_{1,q}$ and ω considered.

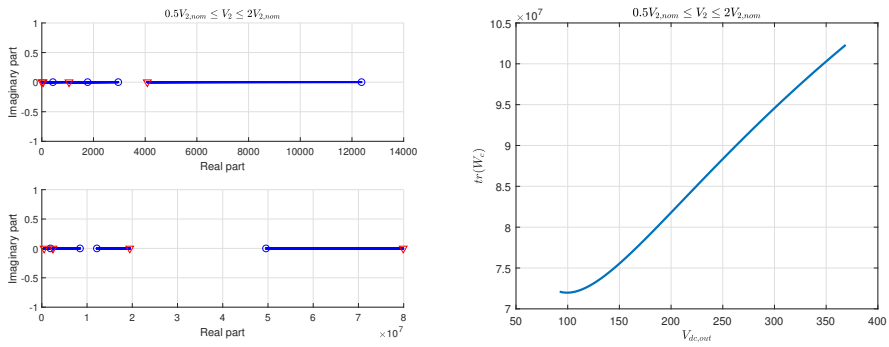

Figure B.3: Eigenvalue trajectories and trace of controllability Gramian with input on both sides, $v_{1,q}$ neglected and ω considered.

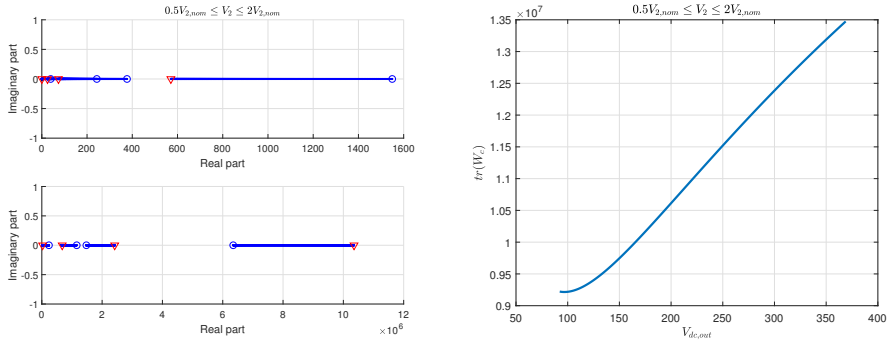

Figure B.4: Eigenvalue trajectories and trace of controllability Gramian with input only on the sending side, $v_{1,q}$ neglected and ω considered.

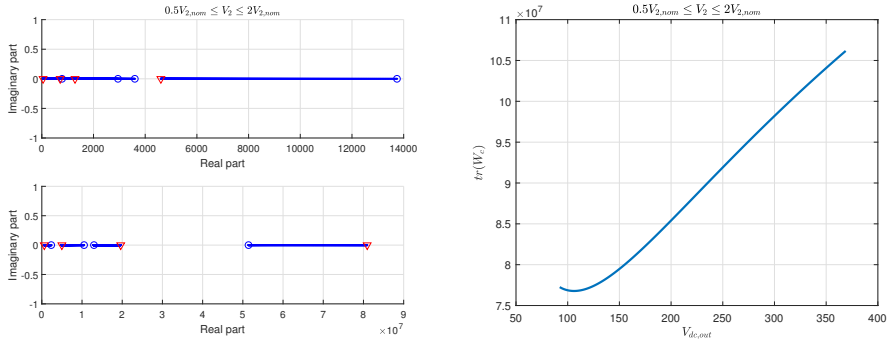

Figure B.5: Eigenvalue trajectories and trace of controllability Gramian with input on both sides, $v_{1,q}$ considered and ω neglected.

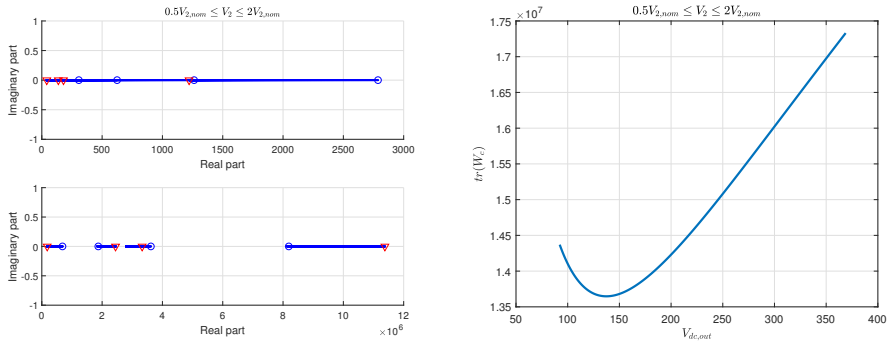

Figure B.6: Eigenvalue trajectories and trace of controllability Gramian with input only on the sending side, $v_{1,q}$ considered and ω neglected.

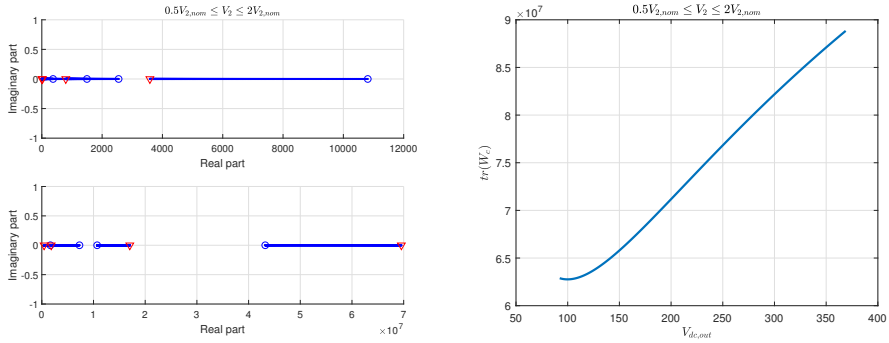

Figure B.7: Eigenvalue trajectories and trace of controllability Gramian with input only on the receiving side, $v_{1,q}$ considered and ω neglected.

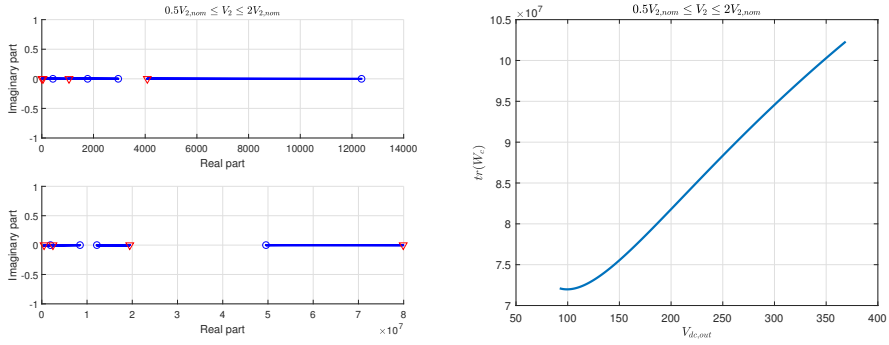

Figure B.8: Eigenvalue trajectories and trace of controllability Gramian with input on both sides, $v_{1,q}$ and ω neglected.

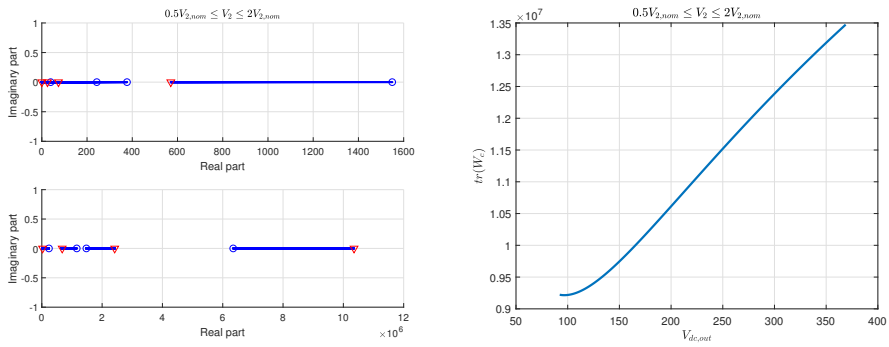

Figure B.9: Eigenvalue trajectories and trace of controllability Gramian with input only on the sending side, $v_{1,q}$ and ω neglected.

B.2 Varying coupling coefficient

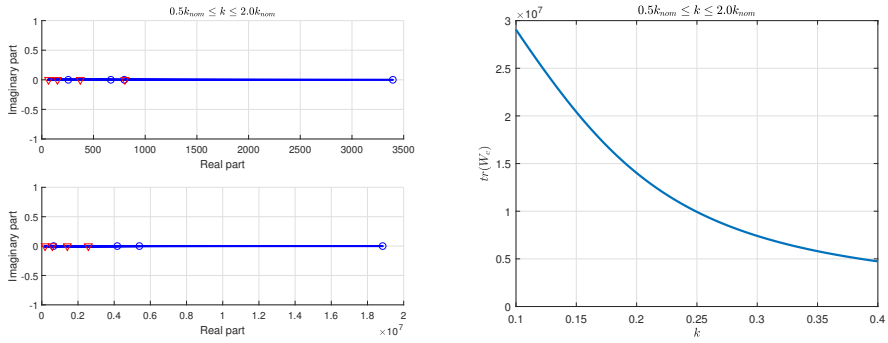

Figure B.10: Eigenvalue trajectories and trace of controllability Gramian with input only on the sending side, $v_{1,q}$ and ω considered.

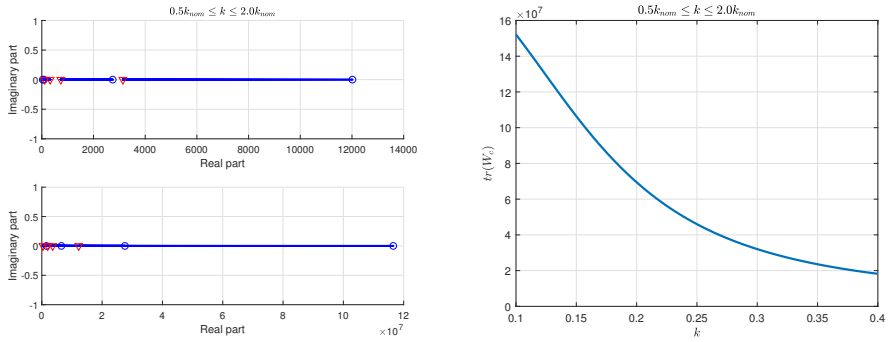

Figure B.11: Eigenvalue trajectories and trace of controllability Gramian with input only on the receiving side, $v_{1,q}$ and ω considered.

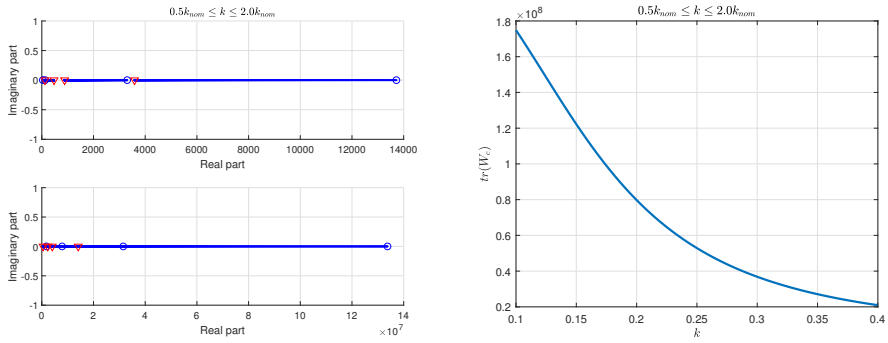

Figure B.12: Eigenvalue trajectories and trace of controllability Gramian with input on both sides, $v_{1,q}$ neglected and ω considered.

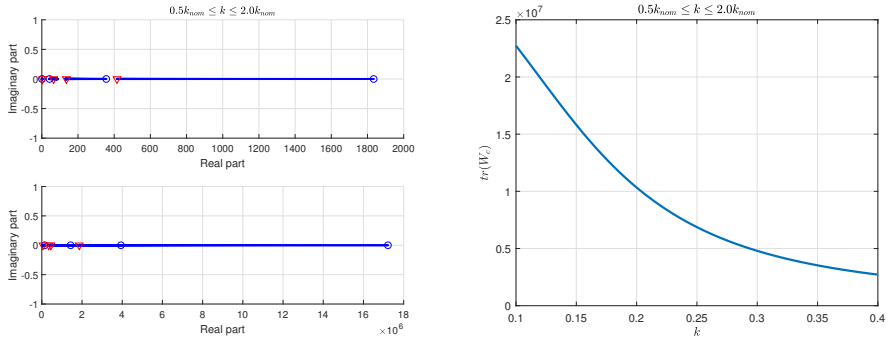

Figure B.13: Eigenvalue trajectories and trace of controllability Gramian with input only on the sending side, $v_{1,q}$ neglected and ω considered.

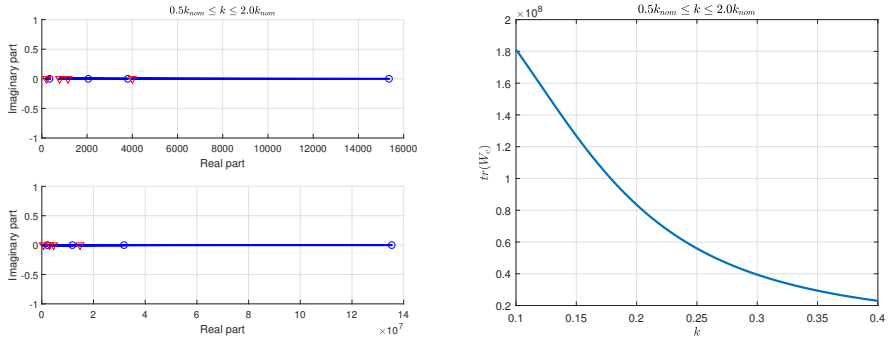

Figure B.14: Eigenvalue trajectories and trace of controllability Gramian with input on both sides, $v_{1,q}$ considered and ω neglected.

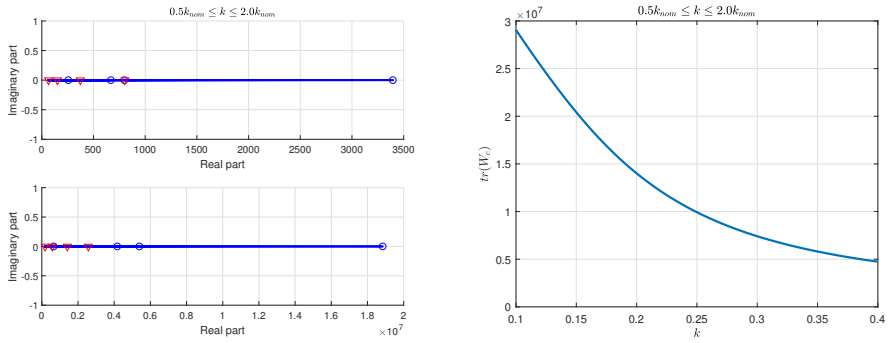

Figure B.15: Eigenvalue trajectories and trace of controllability Gramian with input only on the sending side, $v_{1,q}$ considered and ω neglected.

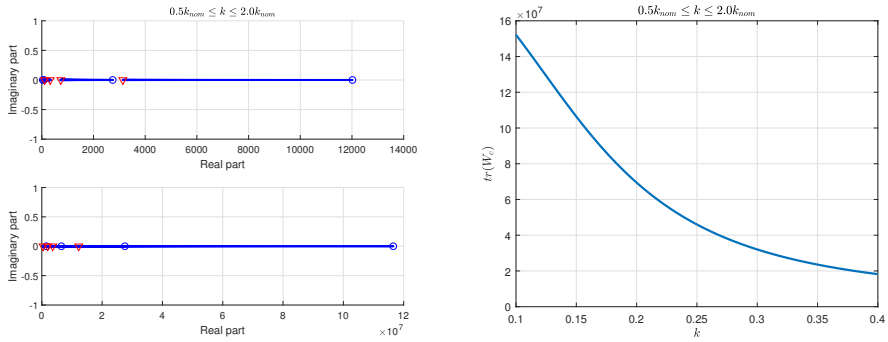

Figure B.16: Eigenvalue trajectories and trace of controllability Gramian with input only on the receiving side, $v_{1,q}$ considered and ω neglected.

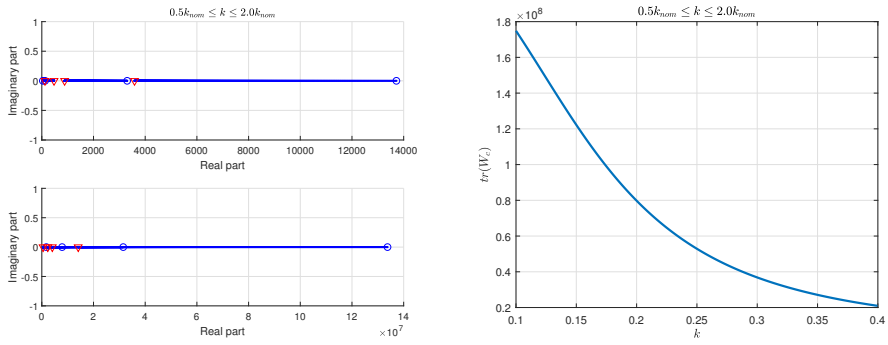

Figure B.17: Eigenvalue trajectories and trace of controllability Gramian with input on both sides, $v_{1,q}$ and ω neglected.

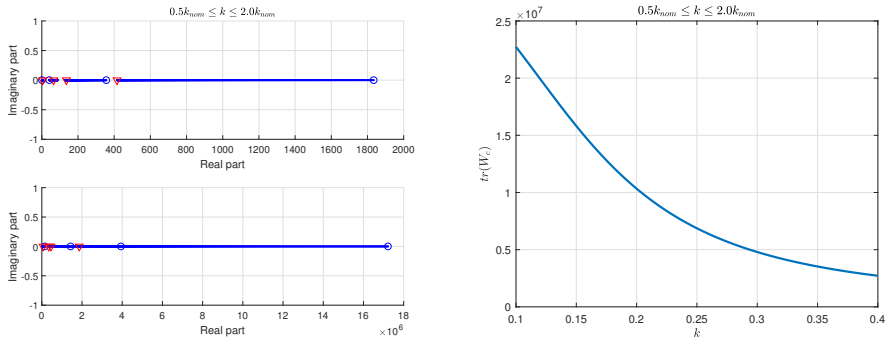

Figure B.18: Eigenvalue trajectories and trace of controllability Gramian with input only on the sending side, $v_{1,q}$ and ω neglected.

Appendix C

Observability Gramian Plots

C.1 Varying load voltage

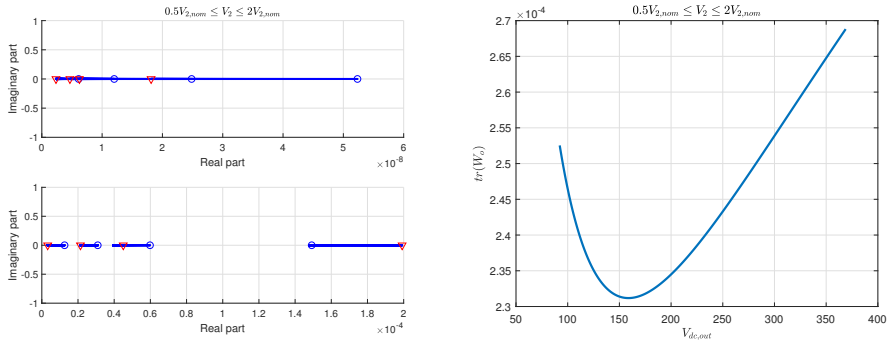

Figure C.1: Eigenvalue trajectories and trace of observability Gramian with measurement on all currents

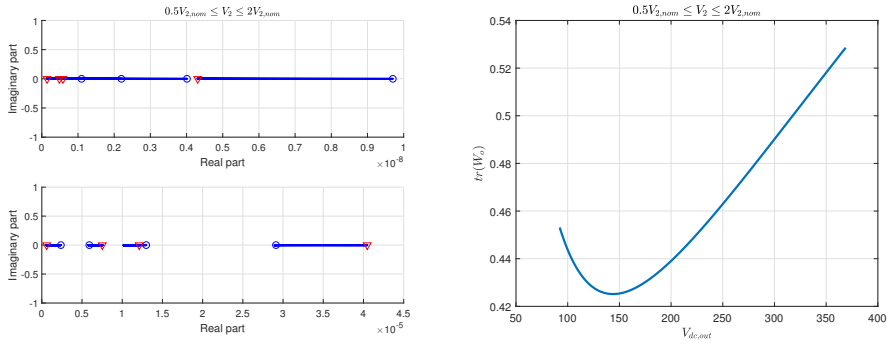

Figure C.2: Eigenvalue trajectories and trace of observability Gramian measurement on sending side currents

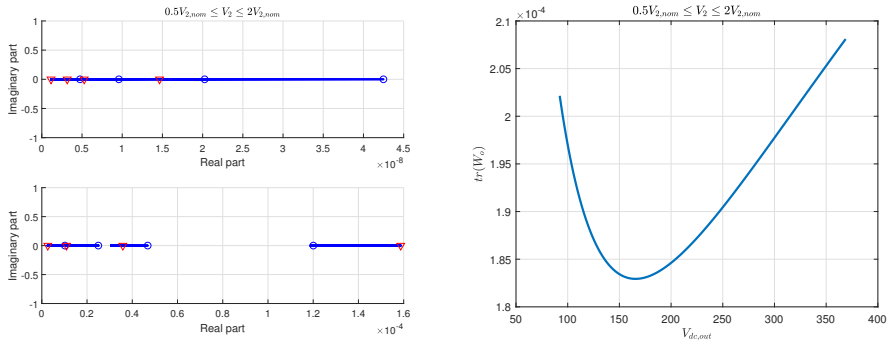

Figure C.3: Eigenvalue trajectories and trace of observability Gramian with measurement on receiving side currents

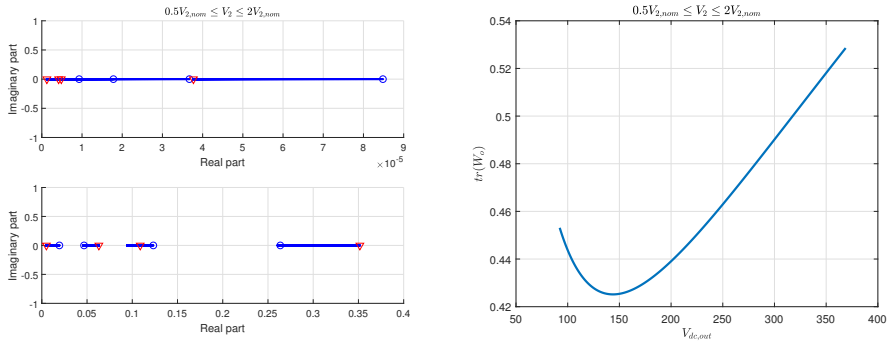

Figure C.4: Eigenvalue trajectories and trace of observability Gramian with measurement on sending side states

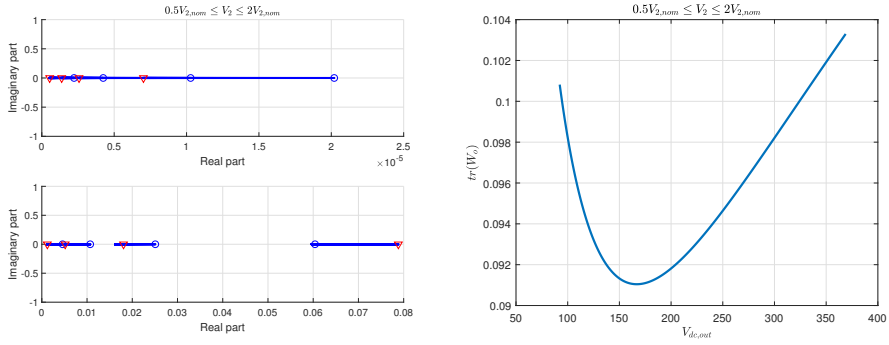

Figure C.5: Eigenvalue trajectories and trace of observability Gramian with measurement on receiving side states

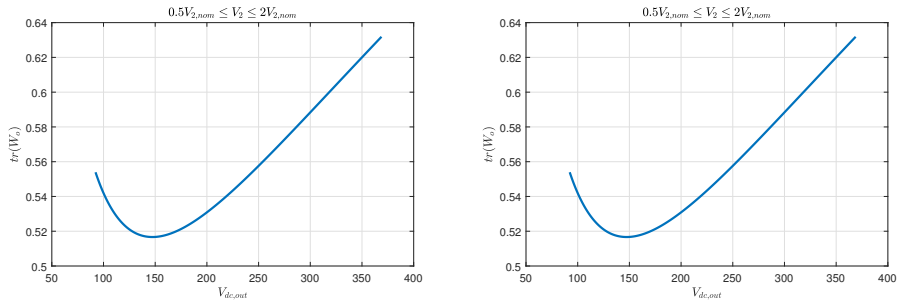

Figure C.6: Eigenvalue trajectories and trace of observability Gramian with measurement on all states

C.2 Varying coupling coefficient

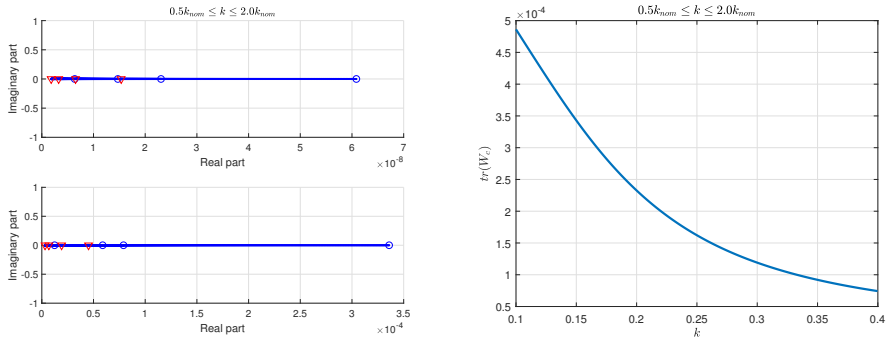

Figure C.7: Eigenvalue trajectories and trace of observability Gramian measurement on all currents

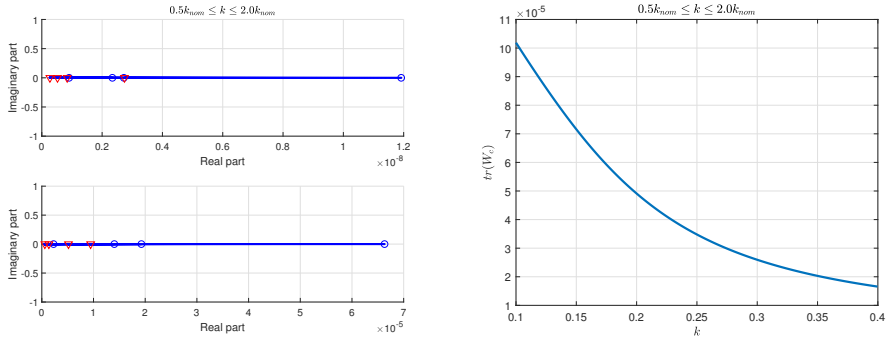

Figure C.8: Eigenvalue trajectories and trace of observability Gramian with measurement on sending side currents

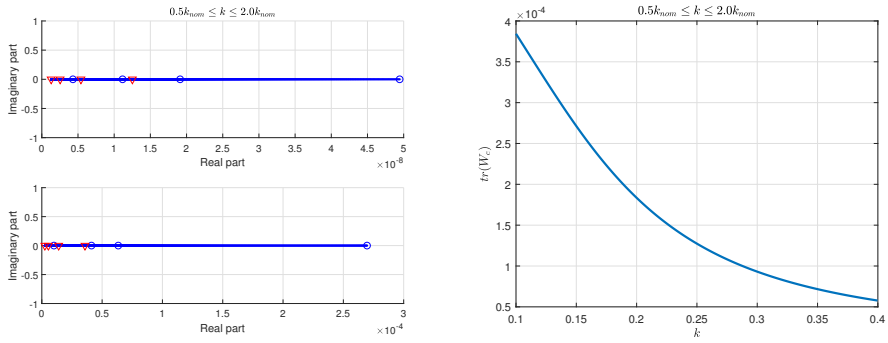

Figure C.9: Eigenvalue trajectories and trace of observability Gramian with measurement on receiving side currents

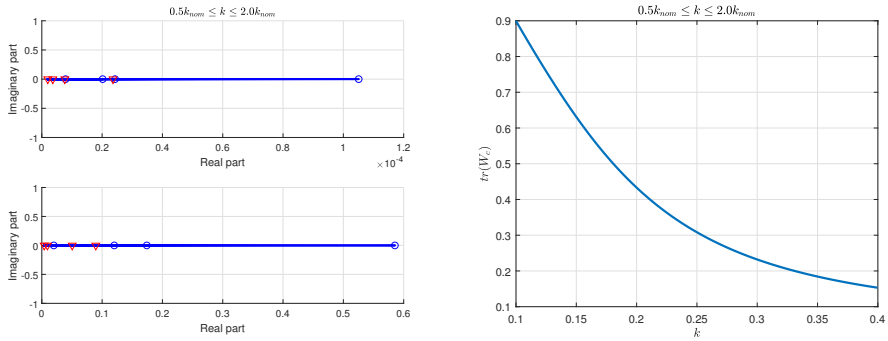

Figure C.10: Eigenvalue trajectories and trace of observability Gramian measurement on sending side states

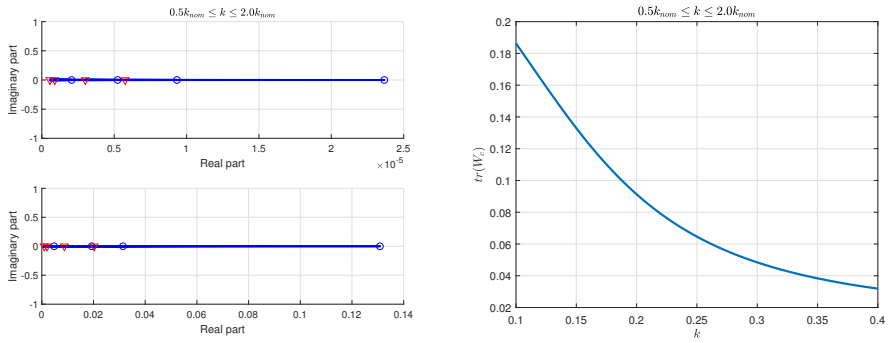

Figure C.11: Eigenvalue trajectories and trace of observability Gramian measurement on receiving side states

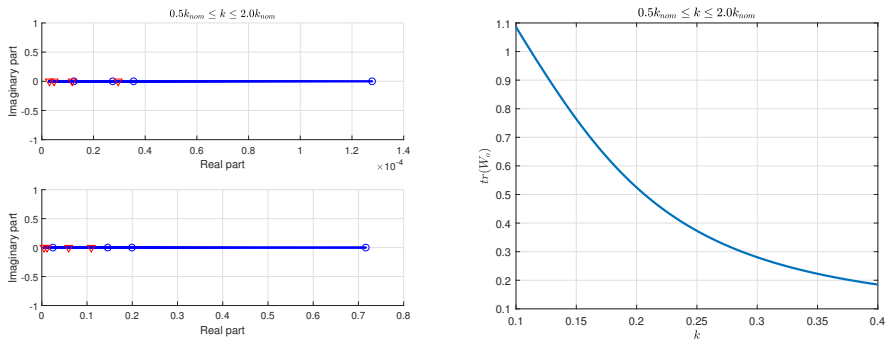

Figure C.12: Eigenvalue trajectories and trace of observability Gramian measurement on all states

Appendix D

Transfer Functions

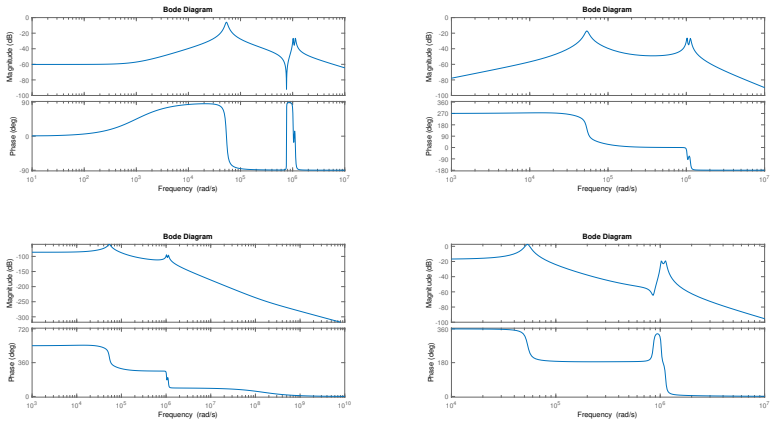

Figure D.1: Frequency response of transfer functions from every input to state $i_{1,d}$. The figures are positioned by rows.

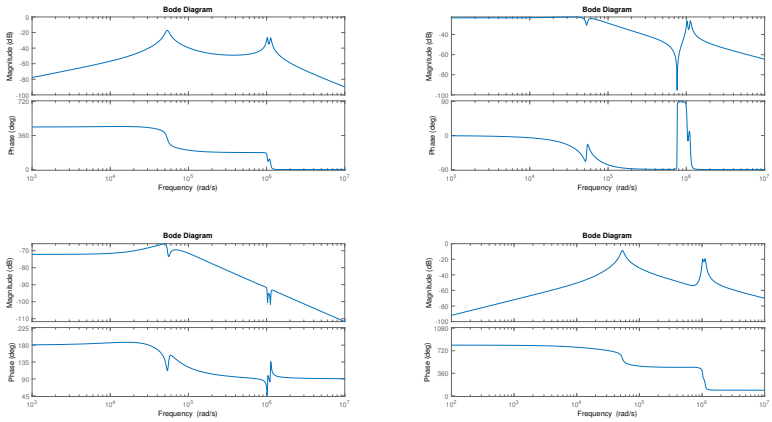

Figure D.2: Frequency response of transfer functions from every input to state $i_{1,q}$. The figures are positioned by rows.

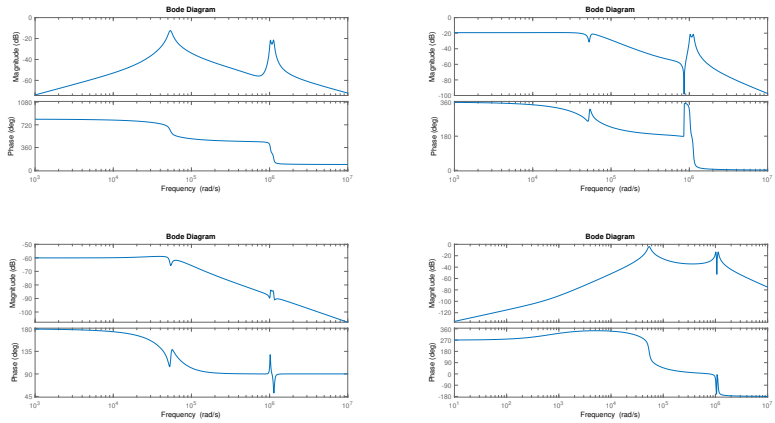

Figure D.3: Frequency response of transfer functions from every input to state $i_{2,d}$. The figures are positioned by rows.

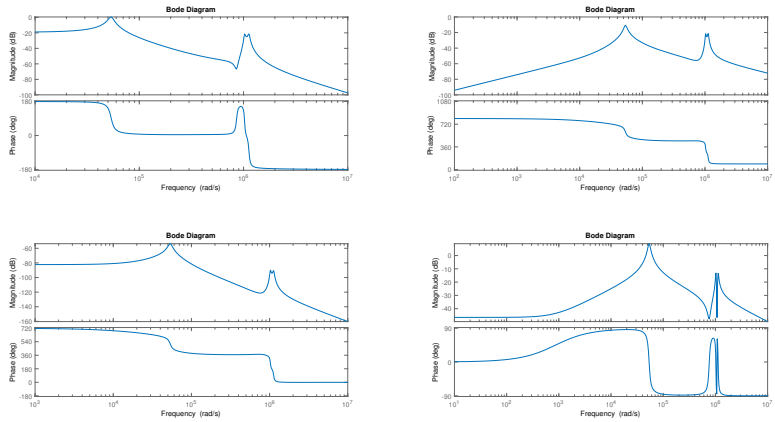

Figure D.4: Frequency response of transfer functions from every input to state $i_{2,d}$. The figures are positioned by rows.

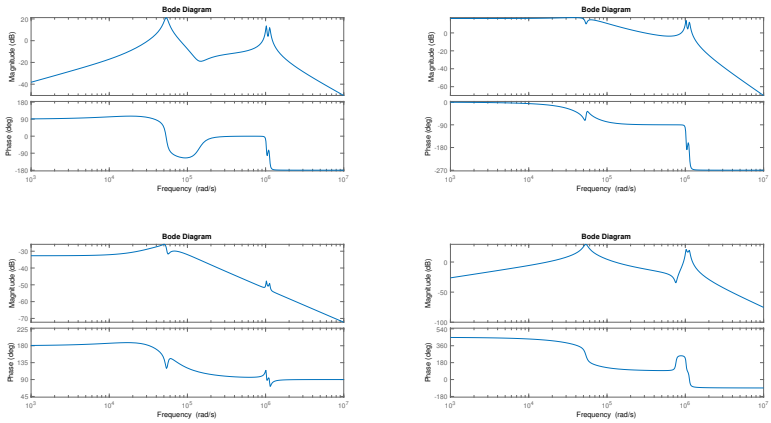

Figure D.5: Frequency response of transfer functions from every input to state $v_{C1,d}$. The figures are positioned by rows.

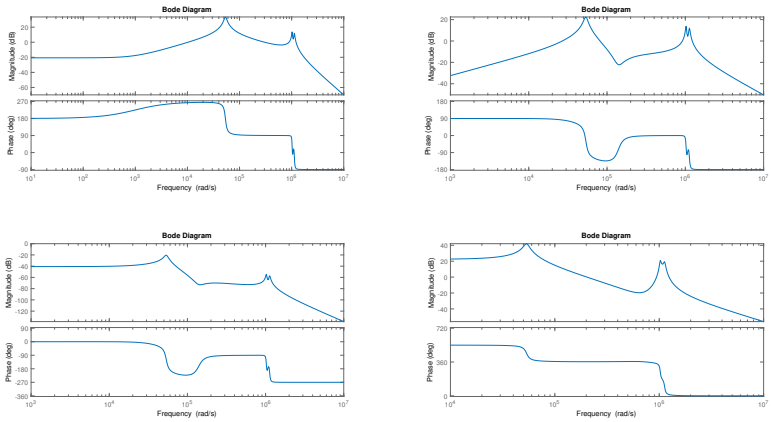

Figure D.6: Frequency response of transfer functions from every input to state $v_{C1,q}$. The figures are positioned by rows.

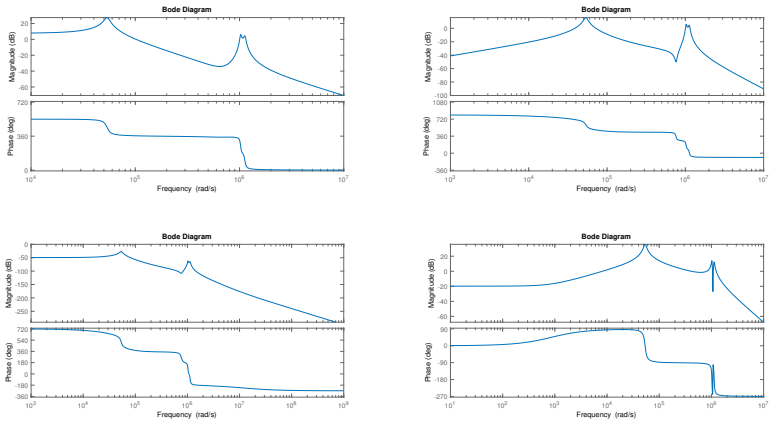

Figure D.7: Frequency response of transfer functions from every input to state $v_{C2,d}$. The figures are positioned by rows.

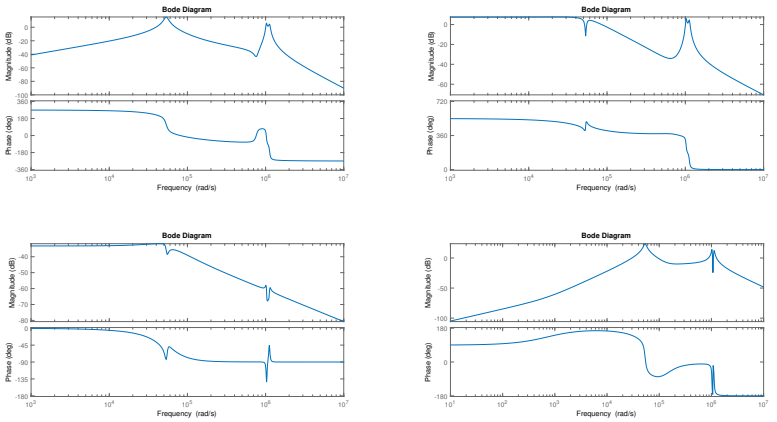

Figure D.8: Frequency response of transfer functions from every input to state $v_{C2,q}$. The figures are positioned by rows.